© 2022. Published by The Company of Biologists Ltd | Biology Open (2022) 11, bio058978. doi:10.1242/bio.058978

METHODS & TECHNIQUES

Myotonic dystrophy type 1 embryonic stem cells show decreased myogenic potential, increased CpG methylation at the *DMPK* locus and RNA mis-splicing

Silvie Franck[1], Edouard Couvreu De Deckersberg[1], Jodi L. Bubenik[2], Christina Markouli[1], Lise Barbé[3], Joke Allemeersch[4], Pierre Hilven[1], Geoffrey Duqué[1], Maurice S. Swanson[2], Alexander Gheldof[1,5], Claudia Spits[1,*] and Karen D. Sermon[1,*,‡]

ABSTRACT

Skeletal muscle tissue is severely affected in myotonic dystrophy type 1 (DM1) patients, characterised by muscle weakness, myotonia and muscle immaturity in the most severe congenital form of the disease. Previously, it was not known at what stage during myogenesis the DM1 phenotype appears. In this study we differentiated healthy and DM1 human embryonic stem cells to myoblasts and myotubes and compared their differentiation potential using a comprehensive multi-omics approach. We found myogenesis in DM1 cells to be abnormal with altered myotube generation compared to healthy cells. We did not find differentially expressed genes between DM1 and non-DM1 cell lines within the same developmental stage. However, during differentiation we observed an aberrant inflammatory response and increased CpG methylation upstream of the CTG repeat at the myoblast level and RNA mis-splicing at the myotube stage. We show that early myogenesis modelled in hESC reiterates the early developmental manifestation of DM1.

KEY WORDS: Myotonic dystrophy type 1, Human embryonic stem cells, Myogenic differentiation, CpG methylation, RNA mis-splicing

INTRODUCTION

Myotonic Dystrophy type 1 (DM1, OMIM# 160900) is caused by an expanded CTG tract in the 3′ untranslated region (3′ UTR) of the *dystrophia myotonica protein kinase* (*DMPK*) gene that mainly affects muscular and neuronal lineages (Brook et al., 1992; Mahadevan et al., 1992; Udd and Krahe, 2012). The unstable CTG repeat continues to expand over the patients' lifetime resulting in somatic mosaicism (Martorell et al., 1997). The longest CTG expansions have been observed in the most severely affected tissues, including muscle, brain and heart (López Castel et al., 2011). Individuals born with very large CTG expansions can manifest congenital DM1 (CDM), which is the most severe form of the disease (De Antonio et al., 2016; Johnson et al., 2016; Nakamori et al., 2017).

DM1 patients experience muscular symptoms such as muscle weakness, myotonia or loss of muscle strength during disease progression (Bouchard et al., 2015). CDM exhibits features that are not seen in adult or classic DM1 patients, including severe muscle fibre immaturity (Farkas-Bargeton et al., 1988; Nakamori et al., 2017; Sarnat, 2011).

At the molecular level, *DMPK* transcripts containing CUG expansions form toxic RNA foci which sequester splicing factors such as muscleblind-like (MBNL) proteins, while also increasing levels of CUG-binding protein 1 (CELF1), leading to altered RNA splicing events causing DM1-related symptoms (Masuda et al., 2012; Wang et al., 2012). In addition, the hypermethylation of the CpG island upstream of the CTG repeat is seen exclusively in CDM patients and has been suggested to be a biomarker for CDM, arguing in favour of its significant contribution to disease severity (Barbé et al., 2017).

The current knowledge of muscle-specific DM1 mechanisms has been obtained from either mouse models, post-mortem human tissues, patient biopsies or tissue-derived myoblasts. Human embryonic stem cells (hESC) have previously been shown to be a suitable model for DM1 (Seriola et al., 2011; Yanovsky-Dagan et al., 2015; Barbé et al., 2017), although the effect of the DM1 expansion on *in vitro* myogenesis from hESC that carry DM1 has not been reported before.

In this study, we modelled early myoblast and myotube development, starting from hESCs, to investigate differences between healthy and DM1 cells. We detected disease-specific mechanisms at early developmental stages and revealed DM1-specific cellular and molecular pathway deregulation over the time course of early myogenic differentiation.

RESULTS

DM1-hESCs differentiate to the myoblast stage, but show a reduced capacity for myotube generation

Six hESC lines were subjected to myogenic differentiation: three non-DM1 cell lines (VUB01, VUB02, VUB06) and three DM1 cell lines (VUB03-DM1, VUB19-DM1, VUB24-DM1), carrying each a differently sized CTG repeat expansion in the *DMPK* locus (Seriola et al., 2011; De Temmerman et al., 2008) (Table 1).

All six hESC lines were differentiated into myoblasts, selected, and from this stock further differentiated three times to

[1]Department Reproduction and Genetics, Vrije Universiteit Brussel, Brussels 1090, Belgium. [2]Department of Molecular Genetics and Microbiology, Center for NeuroGenetics and the Genetics Institute, University of Florida, College of Medicine, Gainesville, FL 32610, USA. [3]Center for Systems and Therapeutics, Gladstone Institutes, San Francisco, 94107 CA, United States. [4]Genomics Core, UZ Leuven, Leuven 3000, Belgium. [5]Center for Medical Genetics, UZ Brussel, Brussels 1090, Belgium.
*Should be considered joint senior authors

‡Author for correspondence (karen.sermon@vub.be)

J.L.B., 0000-0001-6575-9817; M.S.S., 0000-0001-6245-5367; C.S., 0000-0002-0187-5138; K.D., 0000-0002-2311-9034

Received 4 August 2021; Accepted 29 November 2021

Biology Open (2022) 11, bio058978. doi:10.1242/bio.058978

Table 1. hESC lines used in this work

Line	Sex	Inheritance	(CTG)n range
VUB02 non-DM1	Male	N/A	No expansion
VUB06 non-DM1	Female	N/A	No expansion
VUB01 non-DM1	Male	N/A	No expansion
VUB03-DM1 (CDM)	Female	Maternal	343-1651
VUB19-DM1 (DM1)	Female	Paternal	347-638
VUB24-DM1 (CDM)	Female	Maternal	162-3604

multinucleated myotubes (van der Wal et al., 2017). We attempted to differentiate VUB24-DM1 three times also; however, only one differentiation experiment yielded enough myotube material for the RNAseq experiments. VUB03-DM1 was differentiated three times independently (subline 1, 2, 3) in order to control for differentiation variability. VUB19-DM1 had the smallest repeat size that increased with only 22 repeats from hESC to myotubes (Jonckheere-Terpstra test, P=0.009), while the repeat in VUB03-DM1 increased with 151 repeats (Jonckheere-Terpstra, test P=0.001). VUB24-DM1 had the largest CTG repeat size and showed the highest size variability (Fig. S1, Table S1).

Transcriptome analysis was carried out by RNA sequencing for all lines at the hESC, myoblast and myotube stage on one sample each. Principle component analysis (PCA) of all samples showed that the myoblast samples clustered apart from myotubes and hESCs, confirming the presence of three different cell identities (Fig. 1A; Fig. S2). In addition, no significant differences based on FDR<0.05 were found when comparing DM1 with non-DM1 samples of the same cell type, including core myogenic regulatory genes *MYOD* and *MYOG*, and loss of markers of undifferentiated state (Fig. 1B).

After the first differentiation step, we found no significant differences in the percentage of C-MET+/HNK− cells in cell cultures by flow cytometry, suggesting that all lines differentiated with similar efficiency (Fig. 1C). We investigated the activation of muscle-related gene sets using gene-set enrichment analysis during the course of differentiation between DM1 and non-DM1 samples. In the differentiation from hESCs to myoblasts, we found 36 muscle-related GO gene sets that were enriched in non-DM1 samples, and 39 that were enriched in DM1 samples, 32 of which were in common (Fig. 1D; full list of pathways in Table S2). The heatmap in Fig. 1E shows the differentially expressed genes of the hallmark gene set 'myogenesis' (of the molecular signatures database). We only included those genes that were significantly differentially expressed in the non-DM1 lines (FDR<0.05 in non-DM1 hESC to myoblast differential gene expression). Table S4 shows all the included genes and their $\log_2$FC and FDR. Overall, both groups show a comparable expression pattern, with both groups similarly inducing muscle-related genes, confirming that DM1 and non-DM1 cell lines undergo the first part of myogenic differentiation with equal efficiency.

We then investigated the second stage of the differentiation from myoblasts towards myotubes and found that DM1 lines showed a statistically lower number of MF20+ cells (t-test, P=0.0003). VUB24-DM1 showed the lowest numbers of positive cells (Fig. 2A, B) and, moreover, VUB24-DM1 myotubes cluster together with the myoblasts in the PCA analysis (Fig. 1B). A gene set enrichment analysis of the differentiation from myoblasts to myotubes, showed 21 GO gene sets that were enriched in DM1 samples, versus 38 that were enriched in non-DM1 samples, of which 20 muscle related GO gene sets were commonly enriched (Fig. 2C; full list in Table S3). Taking into account the genes from the hallmark gene-set 'myogenesis', there is a considerable number of genes that are not significantly induced in the DM1 group, which are highly induced in the non-DM1 group (Fig. 2D; Table S5).

Inflammatory pathways and mTORC1 signalling are differentially activated during the myogenic differentiation of DM1 hESC

In order to further explore transcriptional differences in the myogenic differentiation we compared the top positively and negatively enriched Hallmark pathways in differential gene expression from hESCs to myoblasts and from myoblasts towards myotubes (Fig. 3). Interestingly, during the differentiation to myoblasts, we found that IL6-JAK-STAT3 signalling and TNFA signalling via NFKB were positively enriched in both experimental groups (Fig. 3A). On the other hand, the interferon alpha response, belonging to interferon type I, was positively enriched in the differentiation of the DM1 hESC to myoblast only. In the second step of differentiation, the interferon type I pathway appears negatively enriched only in the DM1 cells (Fig. 3A). Remarkably, the canonical WNT pathway was only activated in the non-DM1 myoblast-to-myotube transition. The mTORC1 signalling, an important pathway in myogenesis, was negatively enriched in both groups in the transition from myoblast to myotube (Rion et al., 2019).

We further investigated these pathways by analysing the expression of all genes in each pathway (as listed in the Hallmark gene sets). Fig. 3B and Fig. S3 show the heatmaps of the $\log_2$FC of all genes in each pathway with an FDR<0.05 in at least one of the groups. Table S6 lists all genes included in the heatmaps and their $\log_2$FC and FDR. Overall, the majority of genes in the three inflammatory pathways (IL6-JAK-STAT3 signalling, TNFA signalling via NFKB and interferon alpha response) are upregulated in the first part of the differentiation, while in the second part most genes are downregulated, and the only pathway showing differences between the two groups is the interferon alpha response.

In the interferon alpha response pathway, 77% of the genes are upregulated in the DM1 samples and 65% in the non-DM1. Of these upregulated genes, 71% were more strongly induced in the DM1 samples. During the second part of the differentiation, the majority of the interferon alpha response genes were downregulated in the DM1 samples while remaining mostly unchanged in non-DM1. These data support the observation that this pathway was specifically enriched in the DM1 samples during the first part of the differentiation.

With regards to the WNT signalling, the heatmap in Fig. 3B does not reveal pronounced differences in terms of significantly differentially expressed genes between the non-DM1 and DM1 samples, suggesting that the differential enrichment predicted by GSEA is likely not of strong biological relevance.

Finally, the mTORC1 shows striking differences between the two groups. The non-DM1 samples downregulate 87% (62/71) genes in the pathway, suggesting that the mTORC1 signalling is being repressed during the transition from myoblast to myotube. Conversely, the DM1 samples only downregulate 19% (14/71) of the genes, potentially unveiling abnormal activation of the mTORC1 signalling in DM1 myotubes.

In sum, the TNFα signalling via NFKB pathways is equally enriched in both groups. Conversely, the interferon alpha response pathway was only enriched in the DM1 samples, with a stronger up- and downregulation of its genes in the course of differentiation. Further, the mTORC1 signalling showed remarkable differences, with the DM1 cells failing to downregulate this signalling pathway during the progression from myoblast to myotube.

Biology Open (2022) 11, bio058978. doi:10.1242/bio.058978

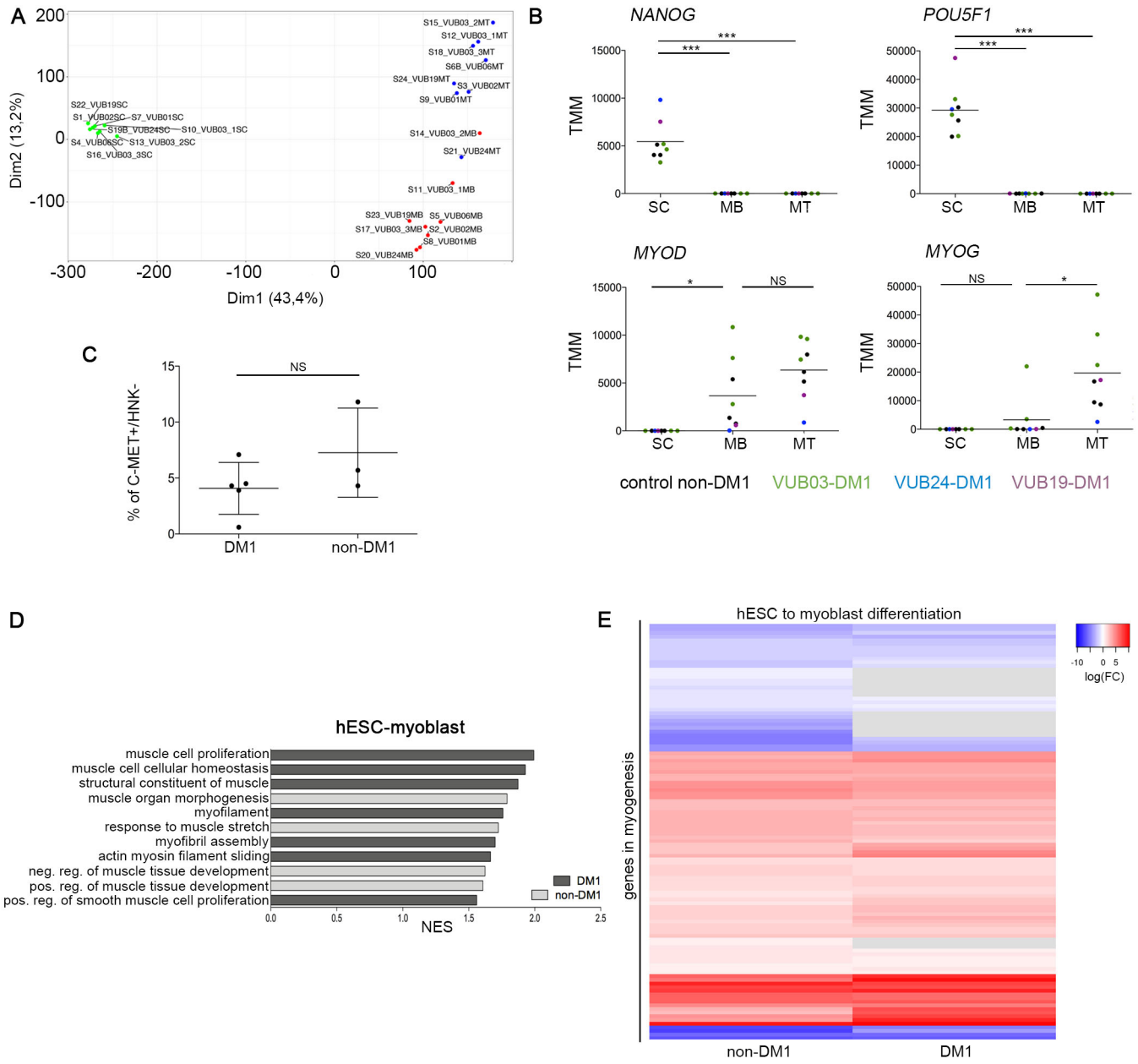

Fig. 1. Myogenic differentiation from hESC to the myoblast stage is equally successful in DM1 and control cell lines. (A) PCA plot of RNA sequencing results of all lines in the undifferentiated state, the myoblast and the myotube stage. The PCA is based on the results for coding genes with a count per million greater than one in at least two samples. (B) Expression of the undifferentiated state markers *NANOG* and *POU5F1*, and myogenic regulatory factors *MYOD* and *MYOG* over the course of myogenic differentiation, as measured by RNA sequencing. (C) Results of the FACS purification of the myogenic differentiation from hESCs towards myoblasts, using a C-MET+ and HNK1– selection for three non-DM1 lines and three DM1 cell lines (one line in triplicate). Data are shown as means±s.d., *t*-test P=0.1935. (D) GO terms for muscle-related gene sets that are significantly enriched in the differential gene expression between hESC and the myoblast stage, using Gene Set Enrichment Analysis. The plot only shows those GO terms that are exclusively enriched for DM1 (dark-grey bars) and non-DM1 (light-grey bars) samples. The full list of 32 commonly enriched gene sets can be found in the Table S2. (E) The heatmap shows the differential gene expression of the genes of the hallmark gene set 'myogenesis' of the molecular signatures database, for DM1 and non-DM1 hESC to myoblast differentiation. Genes in grey have an FDR>0.05. The grey bars indicate genes for which the expression level did not change between two developmental stages. The full list of included genes can be found in the Table S4. N/A, not applicable; ND, not determined; NS, not significant; TMM, trimmed mean of M values; SC, human embryonic stem cells; MB, myoblasts; MT, myotubes; FC, fold change; NES, normalized enrichment score.

CpG methylation upstream of the CTG repeat increases over DM1 myogenic differentiation

We analysed the methylation status of 23 CpG sites upstream of the CTG repeat, including the CTCF1 region, and 11 downstream CpG sites, spanning the CTCF2 region, in all lines included in this study, at the three stages of differentiation, hESCs, myoblasts and myotubes (Fig. 4).

In the undifferentiated state, two of the three DM1 lines showed methylated alleles for the upstream site, while the third line (VUB19-DM1) showed no methylation, as do the control lines.

Biology Open (2022) 11, bio058978. doi:10.1242/bio.058978

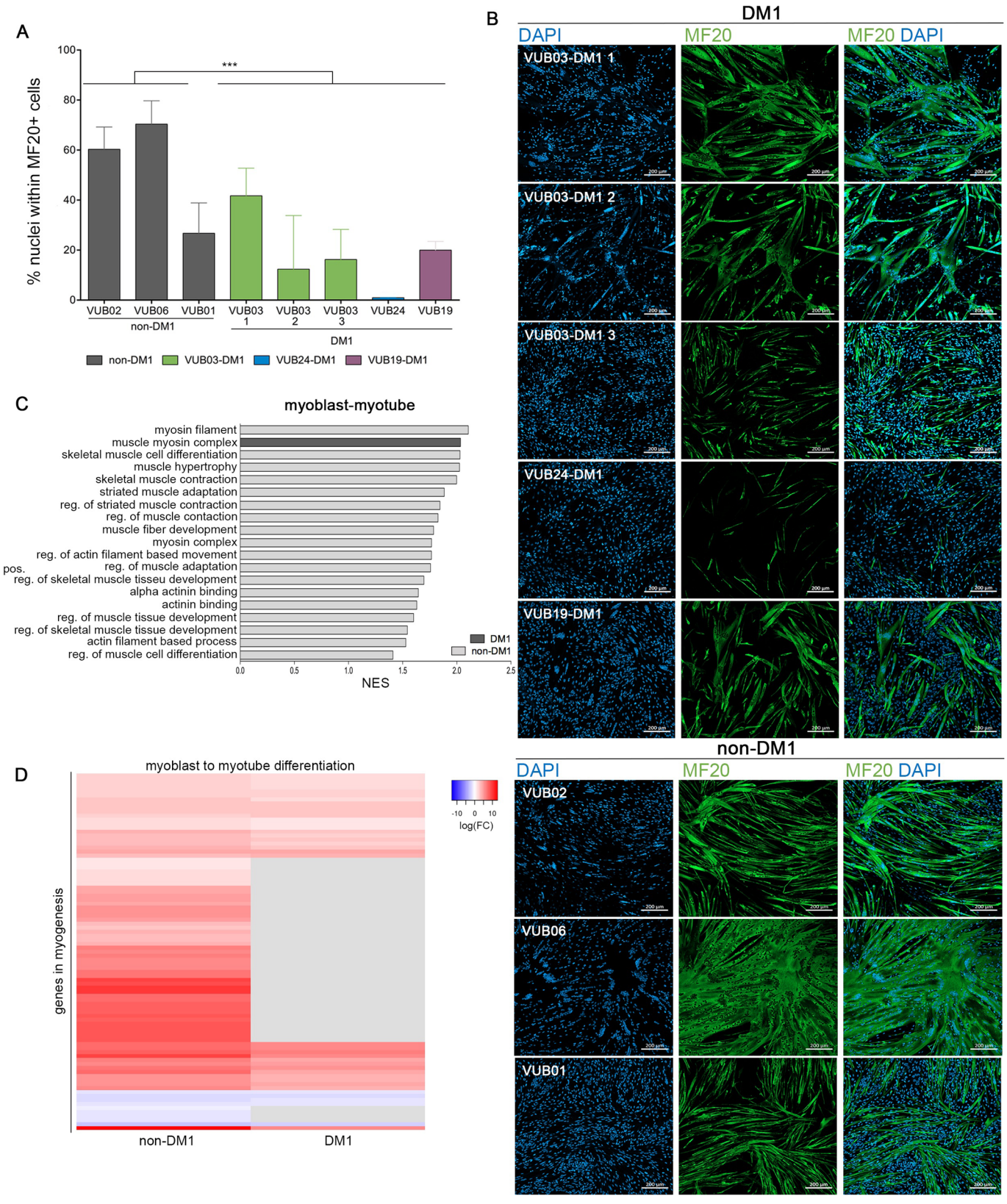

Fig. 2. See next page for legend.

VUB03-DM1 and VUB24-DM1 carry expansions up to 1600 and 3600 repeats, respectively, while the largest expansions in VUB19-DM1 are only 600 repeats (Table 1; Fig. S1). Conversely, at the downstream site all DM1 hESC lines showed methylation and all controls were fully unmethylated (Fig. S4) and this remained unchanged over time and differentiation.

The methylation levels located upstream of the CTG repeat, however, significantly increased in the course of myogenic

Biology Open (2022) 11, bio058978. doi:10.1242/bio.058978

Fig. 2. Myoblasts obtained from DM1-hESC have a decreased ability to progress to the myotube stage. (A) Percentage of nuclei within a myosin heavy chain (MF20) positive myotube (n=3). *** P=0.0003, t-test. (B) Immunostaining for myosin heavy chain (MF20) for three control non-DM1 cell lines and three DM1 cell lines after myotube differentiation. (C) GO terms for muscle-related gene sets that are significantly enriched in the differential gene expression between the myoblast and myotube stage, using Gene Set Enrichment Analysis. The plot only shows those GO terms that are exclusively enriched for DM1 and non-DM1 samples. The full list of gene sets, including 20 common pathways, can be found in Table S3. (D) The heatmap shows the differential gene expression the hallmark gene set 'myogenesis' of the molecular signatures database, for DM1 and non-DM1 myoblast to myotube differentiation. Genes in grey have an FDR>0.05. The grey bars indicate genes for which the expression level did not change between two developmental stages. The full list of included genes can be found in the Table S5. NES, normalized enrichment score; MB, myoblasts; MT, myotubes; FC, fold change.

differentiation in those lines that already had methylation at their undifferentiated state (Fig. 4, one-way ANOVA, VUB03-DM1 and VUB24-DM1 P<0.0001, VUB19-DM1 P=0.2989, VUB02 P=0.7107, VUB06 P=0.3262, VUB01 P=0.9774).

Since brain tissue is also affected by DM1 and is known to be hypermethylated in DM1 patients (López Castel et al., 2011), we differentiated the three DM1 lines and two controls towards neuroectoderm as an early developmental stage of nervous tissue.

Neuroectoderm was obtained after 12 days of differentiation as described in Chetty et al. (2013). All DM1 and non-DM1 hESCs differentiated towards neuroectoderm, as indicated by the presence of high levels of the neuroectoderm marker *PAX6* with immunocytochemistry (Fig. S5A) and RT-qPCR (Fig. S5B). As in myogenic cells, a significant increase in methylation of the CpG region upstream of the repeat was observed for VUB03-DM1 1 and VUB24-DM1 (one-way ANOVA, P<0.0001, Fig. S6A). The methylation profile of VUB19-DM1 and non-DM1 lines VUB06 and VUB01 remained unmethylated in both cell types (one-way ANOVA, P=0.6355, P=0.5681, P=0.1439, Fig. S6A), while the downstream CpG region remained unchanged (Fig. S6B).

Finally, it has been suggested that an aberrant methylation pattern upstream of the CTG repeat might deregulate the chromatin structure and gene expression at the *DMPK* locus (Furling et al., 2001a; Salvatori et al., 2005; Yanovsky-Dagan et al., 2015). Therefore, we assessed the expression of *DMPK*, *SIX5* and *DMWD* over the full myogenic differentiation process for the samples with and without methylation (VUB03 and VUB24 versus VUB19, VUB01, VUB02 and VUB06, Fig. 4B). The levels of *DMPK* and *DMWD* expression increased over the course of differentiation, and *SIX5* stayed relatively stable, but none significantly differed between methylated and non-methylated samples.

In conclusion, upstream methylation increases upon myogenic as well as neurogenic differentiation in our DM1 samples with the largest repeats and pre-existing methylation, without apparently affecting the expression of *DMPK* and its flanking genes.

DM1 relevant splicing defects appear in the myotube stage

RNA mis-splicing is widespread in DM1 and is primarily driven by the sequestration of MBNL proteins on the CUG expanded DMPK transcripts and an increase in CELF1 levels. We first compared the RNA levels for these factors across myogenic differentiation in both non-DM1 and DM1 cell lines. There were no significant differences based on disease status, however, the levels were modulated by differentiation state (Fig. 5A).

We analysed RNA alternative splicing switches during myogenic differentiation and compared these profiles between the non-DM1 and DM1 lines.

First, we analysed splicing changes in response to differentiation. Unsurprisingly there were many developmentally regulated alternative splicing switches with similar numbers of splicing changes in both the non-DM1 and DM1 cell lines (Fig. 5C). The transition from hESC to myoblast displayed 2967 events in DM1 and 2874 events in non-DM1 lines, while the myoblast to myotube switch resulted in 1510 and 1640 events, respectively. We then examined differences between disease and control samples at each of the developmental points, and found 231 differential splicing events in hESCs, 239 in myoblasts and 261 in myotubes (Fig. 5B).

Several previous studies have examined DM1 mis-splicing events in various contexts (Jenquin et al., 2019; Nutter et al., 2019; Thomas et al., 2017; Wagner et al., 2016). Within our dataset, previously identified DM1-associated events were predominantly found at the myotube stage and examples include *ARHGEF10L*, *BIN1*, *TNNT3*, *NCOR2*, *NUMA1*, *MBNL1*, *GOLGA4*, and *MEF2C* (Fig. 6A) though *CDK10* and *MACF1* were already present at the myoblast stage. In addition, transcripts for *INSR* and *SEMA6C* started to appear in non-DM1 samples but were absent in DM1 samples at this stage. The difference in repeat length across our three DM1 hESC lines introduces additional variability into the splicing data, and when we perform the same analysis with the VUB03 sublines only, more DM-1 associated events are detected. These events are trending similarly in the complete set but are unable to pass the filter cut-off due to larger variance in the $|\Psi|$ or FDR values. In addition to these previously identified DM1-associated events, we observed that *PARP2*, *SLC3A2*, *METTL2B* and *CPNE1* all contained alternative splicing events that already occur in hESCs but the potential impact of these differences on disease or differentiation remains to be elucidated. Additional significant DM1-specific mis-splicing events in *LDB3*, *MACF1*, *NDUFV3*, *SLAIN2* and *SORBS1* appeared in the myotube stage.

Over the full time course of myogenic differentiation, we were able to follow a few DM1-specific skipped exon transcripts. Transcripts for *CAMK2G*, *NCOR2* and *MBNL1* seem to follow the same trend during differentiation in DM1 and non-DM1 samples (Fig. 6B). In contrast, *FN1ex25*, *GOLGA4ex23*, *NCOR2ex45* and *HOOK3ex2* follow the same trend from ESCs to myoblasts but show a different behaviour between DM1 and non-DM1 samples at the myotube stage (Fig. 6B). For *HOOK3ex2* the splice isoform persists in the DM1 myotubes while disappearing in the non-DM1 myotubes, while the reverse holds for *FN1ex25*, *GOLGA4ex23*, and *NCOR2ex45*, confirming the data obtained comparing mis-splicing between DM1 and non-DM1 within cell types (Fig. 6A), i.e. that splicing differences between DM1 and non-DM1 samples start to appear at the myotube stage. Tables S7–14 show the comparisons between non-DM1 and DM1 samples, as well as between different differentiation stages. The data were filtered with thresholds averaging five reads or greater, 10% change in splicing, and FDR<0.05.

DISCUSSION

In this report we investigated the first steps in the DM1 disease process using hESCs that naturally carry the DM1 mutation with a focus on early myogenic differentiation. We found that while both DM1 and non-DM1 lines equally differentiated to the myoblast stage, DM1 cells less efficiently underwent further maturation to myotubes. This observation may reflect the immature muscle phenotype seen in DM1 patients (Nakamori et al., 2017).

Biology Open (2022) 11, bio058978. doi:10.1242/bio.058978

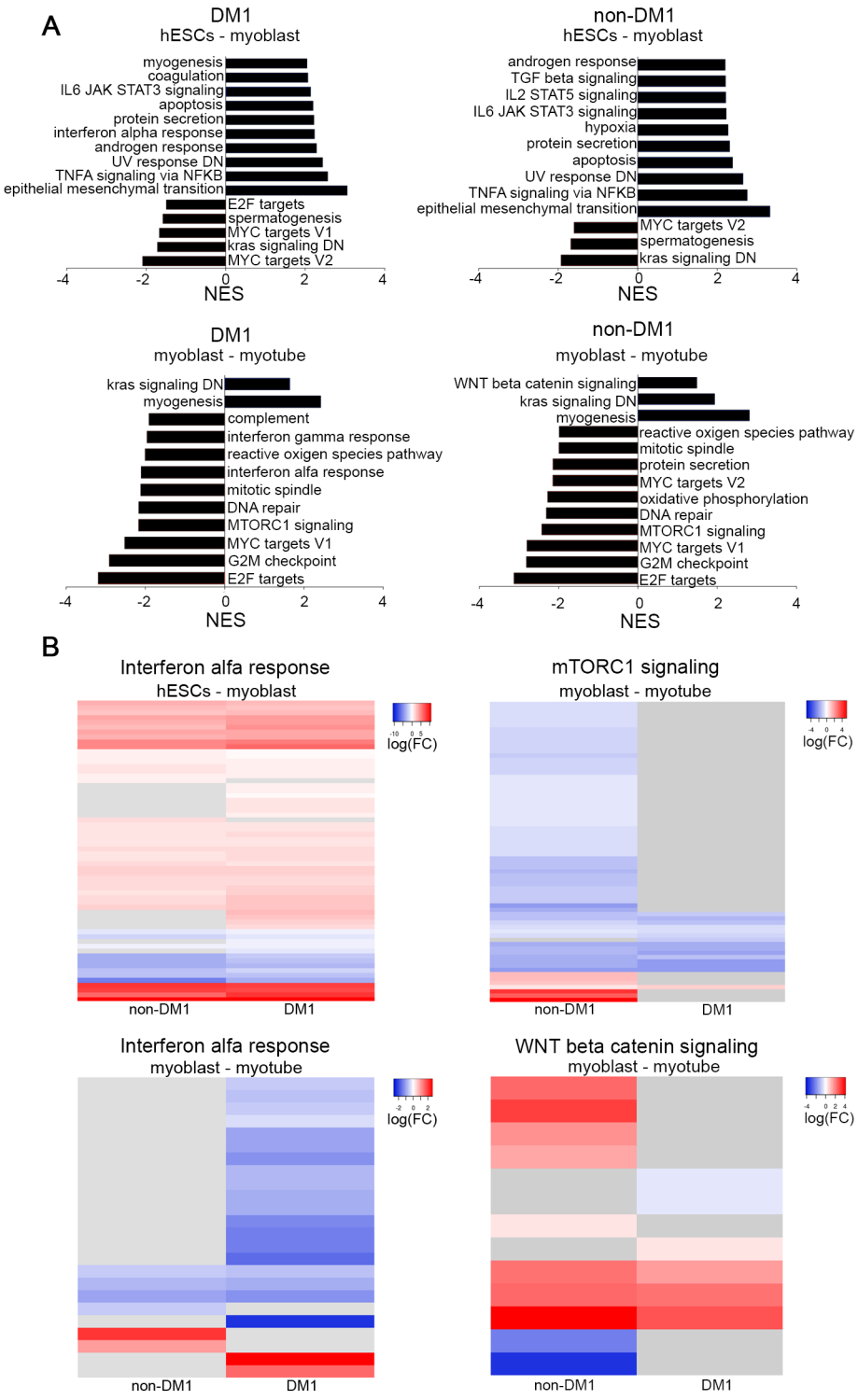

Fig. 3. Pathway analysis in DM1 and non-DM1 samples during myogenic differentiation shows differences in inflammatory response and mTORC1 signalling. (A) Top ten up- and downregulated pathways. The top panel presents myoblasts compared to hESC, the lower panel represents myotubes compared to myoblasts. (B) Heatmaps representing the log fold change of genes belonging to the interferon alpha response, mTORC1 and canonical WNT signalling. The grey bars indicate genes for which the expression level did not change between two developmental stages. The full list of genes, their log2FC and FDR are listed in Table S6. Grey lines indicate genes with FDR>0.05. NES, normalized enrichment score; FC, fold change.

While some reports show that cells with a repeat size in the CDM range do not always display an impaired differentiation potential (Loro et al., 2010; Rizzo et al., 2018) and that removal of CTG repeats by CRISPR/Cas9 does not change the capacity of the cells to form myotubes (Provenzano et al., 2017), others report an increased fusion capacity in repeat-deleted cells (van Agtmaal et al., 2017). In our hands, expanded repeats retain their unstable character during myogenic differentiation but we were not able to demonstrate a correlation between large CTG repeats and differentiation potential.

Another aspect we investigated is the activation of specific inflammatory pathways in the course of differentiation. Proinflammatory factors like IL6 and TNFA are necessary for the proliferation of muscle progenitor cells while suppressing further muscle differentiation (Otis et al., 2014), which is in line with these pathways being positively enriched in the first part of differentiation, and negatively enriched in the second part, both for DM1 and non-DM1 hESC lines. Conversely, abnormal activation of the IL6-STAT3 signalling pathway via the activation of NFKB has been proposed as an underlying cause of the immature

Biology Open (2022) 11, bio058978. doi:10.1242/bio.058978

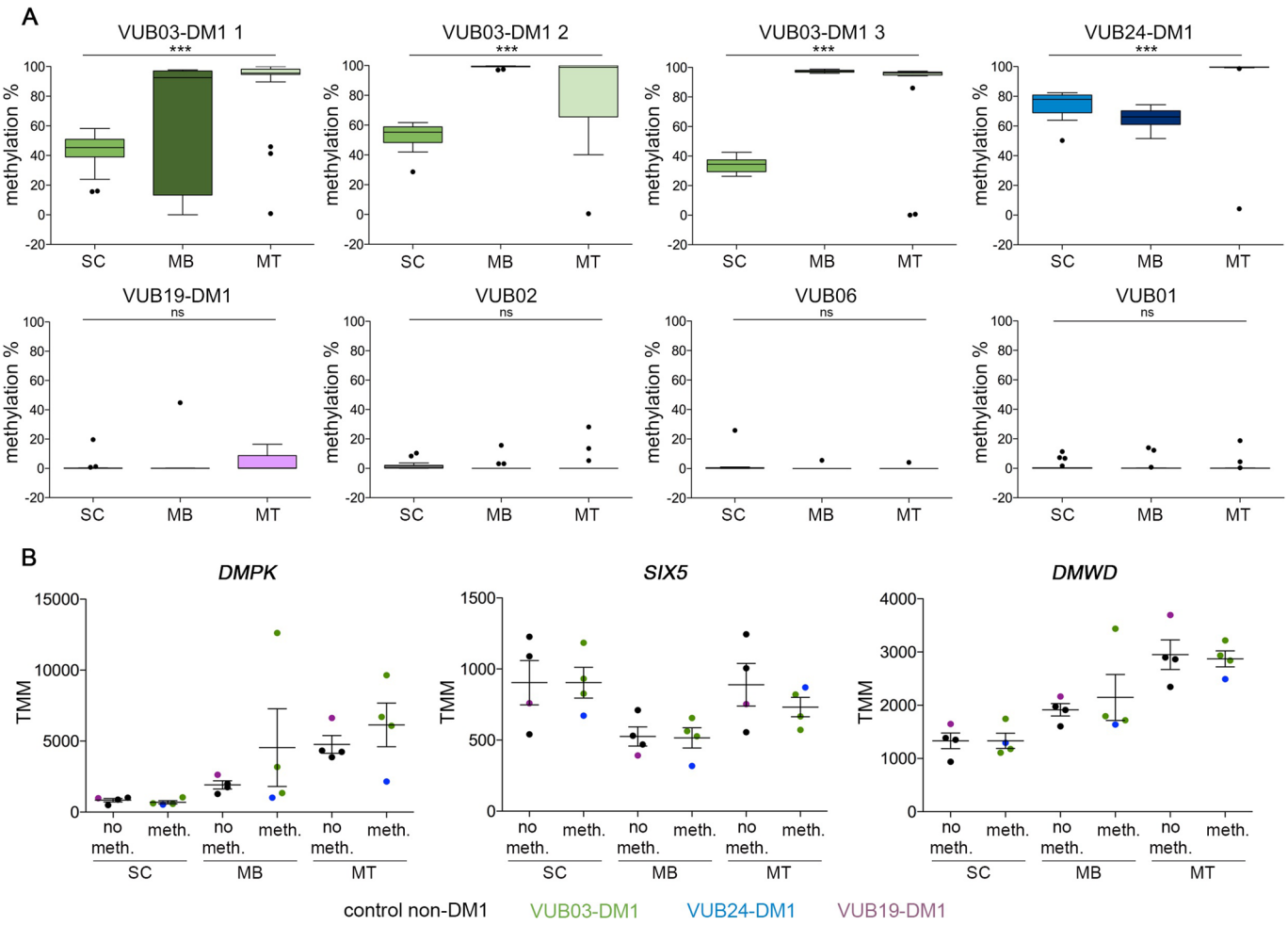

Fig. 4. The upstream CpG methylation in the *DMPK* locus increases over differentiation in DM1 samples but does not affect the expression of *DMPK* and its flanking genes. (A) Average methylation levels of the CpG sites upstream of the CTG repeat in each sample. The upstream methylation is shown for 23 CpG sites and all epi-alleles were analysed after massive parallel sequencing for three DM1 and three non-DM1 cell lines (one-way ANOVA: VUB03-DM1 1: $P<0.0001$ 2: $P<0.0001$ 3: $P<0.0001$, VUB24-DM1: $P<0.0001$, VUB19-DM1: $P=0.2989$, VUB02: $P=0.710$, VUB06: $P=0.326$, VUB01: $P=0.977$; *** indicates significant differences). (B) mRNA levels of *DMPK*, *SIX5* and *DMWD* over the course of myogenic differentiation. Samples are grouped according to their CpG methylation status upstream of the CTG repeat. Data are presented as mean±s.e.m. TMM, trimmed mean of M values; SC, hESC; MB, myoblasts; MT, myotubes.

muscle state observed in CDM (Nakamori et al., 2017). These authors proposed that hypermethylation upstream of the CTG repeat deregulates *DMPK* transcription resulting in a higher level of toxic RNA, which leads to activation of the IL6 pathway. Recently, activation of the interferon type 1 (IFN1) pathway was also shown to be involved in impaired myogenesis and was suggested to be activated by the toxic RNA foci (Rizzo et al., 2018). In our model, we found that IL6-JAK-STAT3 signalling and TNFA signalling via NFKB were positively enriched in both experimental groups, albeit that the IL6-JAK-STAT3 signalling may have been more strongly upregulated in the control group, while the interferon alpha response was exclusively enriched in the DM1 cells. Given that the IFN1 response has been associated with an inhibition of myogenesis (Rizzo et al., 2018), its strong induction in the myoblast stage may be partially responsible for the poorer myotube formation in the DM1 cell lines. A sustained proinflammation signal in the beginning of myotube formation may hamper further myogenic differentiation (Dort et al., 2019), resulting in the observed decreased efficiency of the DM1 cells to generate myotubes.

Our model potentially also confirmed the involvement of mTORC1 in myogenesis (Rion et al., 2019) as well as in DM1 muscle pathology. Brockhoff et al. (2017) demonstrated in a DM1 mouse model that mTORC1 signalling remained active in mutant mice subjected to starvation, while mTORC1 signalling becomes inactive in normal mice (Brockhoff et al., 2017). In our model, while mTORC1 signalling was comparably active in myoblasts (data not shown), it was clearly downregulated in non-DM1 myoblasts differentiating towards myotubes, while this was not the case in DM1 myotubes. Whether mTORC1 is activated (Brockhoff et al., 2017) or on the contrary inhibited (Beffy et al., 2010; Denis et al., 2013) in DM1 remains a topic of controversy. However, further functional experiments in our model would contribute to help unravel the exact role of mTORC1 signalling in DM1 myogenesis.

Muscle tissue from DM1 patients and fetuses, and isolated DM1 myoblasts and myotubes, are known to display high levels of methylation on the CpG island upstream of the CTG repeat (López Castel et al., 2011; Nakamori et al., 2017; Rizzo et al., 2018) and muscle immaturity itself has suggested to be linked to hypermethylation of this site (Nakamori et al., 2017). In our model we showed that the CpG methylation increased over myogenic differentiation, especially in those hESC lines that

Biology Open (2022) 11, bio058978. doi:10.1242/bio.058978

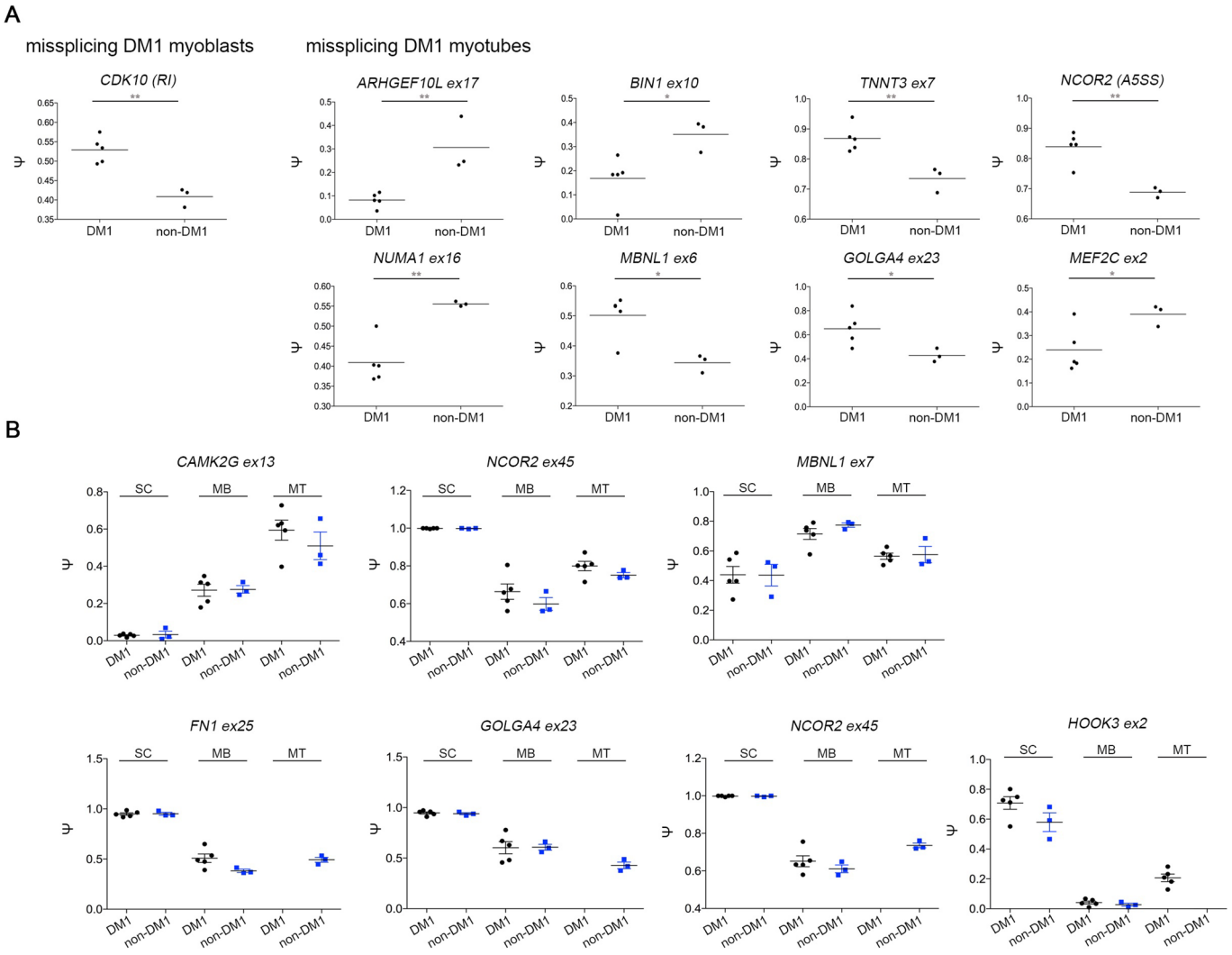

Fig. 5. Expression profile of splicing factors and splicing events in DM1 and non-DM1 hESC, myoblasts and myotubes. (A) Expression levels of the MBNL-like mRNAs and CELF1 for hESCs, myoblasts and myotubes and for DM1 and non-DM1 samples. (B) Differential splicing events in DM1 hESCs, DM1 myoblasts and DM1 myotubes versus their non-DM1 counterparts. Dot plots were created based on ΔΨ and filtered for number of reads ≥5, FDR ≤0.05 and |ΔΨ|>0.1. (C) Differential splicing events over differentiation from hESCs to myoblasts and from myoblasts to myotubes for DM1 and non-DM1 samples. Dot plots were created based on ΔΨ and cut off values number of reads ≥5, FDR ≤0.05 and |ΔΨ|>0.1. TMM, trimmed mean of M values; SC, hESC; MB, myoblasts; MT, myotubes, A3SS, alternative 3′ splice site; A5SS, alternative 5′ slice site; MXE, mutually exclusive exon; RI, retained intron; SE, skipped exon.

already showed hypermethylated in the undifferentiated state and which displayed the largest repeat sizes, confirming previous reports indicating that upstream methylation is associated with large CTG repeats and congenital DM1 (Barbé et al., 2017; Yanovsky-Dagan et al., 2015). In line with the published results on CDM1 fetal and newborn myoblasts, we found that this increased methylation is already established at the myoblast stage and even further increases during differentiation to the myotube stage.

It has been suggested that hypermethylation of the *DMPK* flanking CpG regions affects the expression levels of flanking genes, *DMWD* upstream and *SIX5* downstream (Brouwer et al., 2013; Eriksson et al., 2001; Yanovsky-Dagan et al., 2015). The expression of *DMPK* has been suggested to be essential in myogenesis and further in muscle function (Carrell et al., 2016). In our study, we could not find a significant difference in expression levels of *DMPK, SIX5* and *DMWD* between lines with hypo- and hypermethylation, nor a correlation between the methylation and the differentiation capacity. This suggests that the methylation status of this region is not controlling the expression of these genes at this stage of myogenesis and is not a likely explanation for the observed differentiation differences between DM1 and non-DM1 cells.

During myogenic development, mRNA alternative splicing transitions are essential for a proper tissue function and muscle physiology (Brinegar et al., 2017). Alternative splicing is misregulated in DM1 and even more so in CDM1 patients leading to developmentally inappropriate RNA isoforms, eventually causing multisystemic DM1 symptoms (Nakamori et al., 2017; Thomas et al., 2017). In a DM1 mouse knock-in model, in which CTG expansions were inserted into the 3′ UTR of the mouse Dmpk gene, Nutter et al. (2019) demonstrated that the expanded CTG repeat has more severe effects on muscle progenitor stages such as myoblasts and myotubes because of the higher expression of Dmpk at those stages and therefore higher capacity to sequester proteins leading to significant RNA mis-splicing (Nutter et al., 2019). Wagner et al. (2016) proposed 46 aberrant splicing events related to

Biology Open (2022) 11, bio058978. doi:10.1242/bio.058978

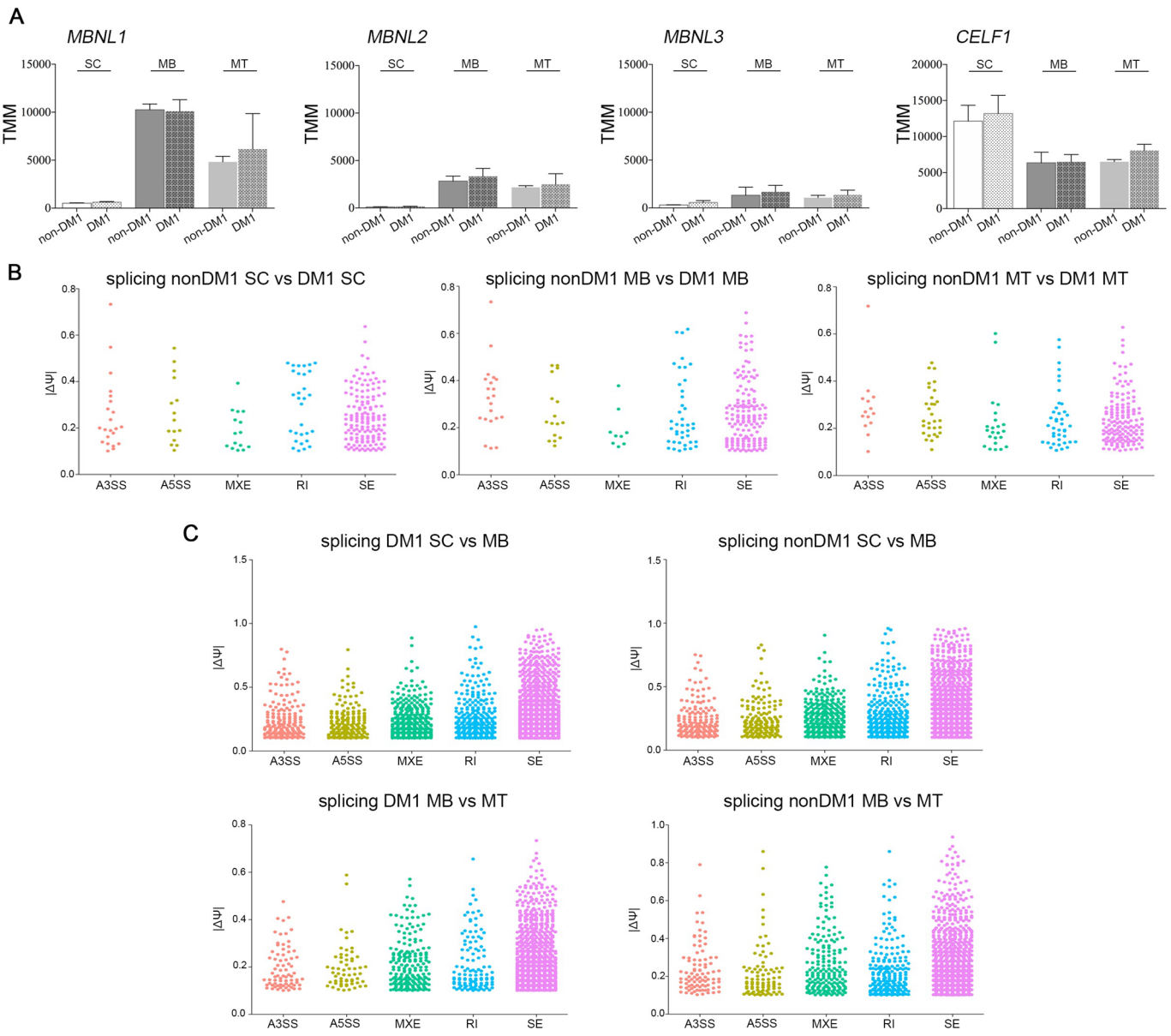

Fig. 6. Specific mis-splicing in DM1 and non-DM1 samples. (A) Mis-splicing in the myoblasts stage and myotubes stage when comparing DM1 and non-DM1 samples. * and ** indicate significantly different results as calculated with *t*-test. (B) Splice variants over differentiation from hESCs to myoblasts and further towards myotubes. No data means no splice variants detected. SC, hESC; MB, myoblasts; MT, myotubes.

DM1 that could serve as DM1 biomarkers (Wagner et al., 2016). We found the majority of the alternative splicing events proposed by Wagner et al. (2016) in our dataset, of which for example *SORBS1*, *NUMA1*, *MBNL1*, *GOLGA4* and *MEF2C* were significantly different to non-DM1 samples at the myotube stage. This indicates that splicing differences only appear from the myotube stage on and therefore mis-splicing might not be the cause of aberrant myogenesis in earlier stages. In addition, we and others showed that *DMPK* levels increase from the myoblast to the myotube stage (Furling et al., 2001b; Wang et al., 2019), likely increasing the mutated, toxic *DMPK* transcript load which could explain why alternative splicing abnormalities become significantly apparent only at the myotube stage.

Mis-splicing of *BIN1* has been linked to T tubule alterations and muscle weakness (Fugier et al., 2011) and was particularly mis-spliced in the poorly differentiating VUB24-DM1 line. This may indicate that a developmental switch to the correct *BIN1* isoform is not only essential postnatally and in adulthood as suggested by others (Fugier et al., 2011) but during early myogenesis as well. More recently, the precise *BIN1* isoform regulation has been shown to be essential for normal muscle development, maturation and function (Cowling et al., 2017; Prokic et al., 2020).

Mis-splicing of *CLCN1*, a skeletal muscle specific chloride channel which causes myotonia (Pistoni et al., 2010), was not identified since *CLCN1* is not yet expressed in these early developmental stages. Interestingly, the insulin receptor (*INSR*) and the sarcoplasmic/endoplasmic reticulum calcium ATPase 1 (*SERCA1*) transcripts which were also suggested to be mis-spliced in DM1 skeletal muscle myotubes (Provenzano et al., 2017), started to appear in myotubes of non-DM1 samples, but failed to do so in non-DM1 samples. Other mis-splicing events such as in *TNNT3*, *MYOM1*, *TNN*, *TRIM55* and *MYO5A* were also observed. Several of these transcripts were linked to actin cytoskeleton and function (Koebis et al., 2011).

Biology Open (2022) 11, bio058978. doi:10.1242/bio.058978

In summary, our findings show that modelling myogenesis using DM1 hESCs recapitulates a number of key cellular and genetic phenotypes that have been previously associated to DM1 pathogenesis. DM1 hESCs have less effective induction of myotube formation than control hESCs, and at the transcriptome level, the model recapitulates previously published observations showing an elevated interferon type I response as an intrinsic feature specific to DM1 myogenesis. We found that myogenic differentiation of DM1 hESC increased already present CpG hypermethylation in the region upstream of the CTG repeat. Finally, we demonstrated that misregulated alternative splicing events start to occur from the myotube stage on, later during myogenic differentiation. We showed that our *in vitro* model is interesting and relevant to study early DM1 pathogenesis and to further unravel abnormal myogenesis.

MATERIALS AND METHODS

Cell culture and skeletal myogenic progenitor differentiation

The VUB hESC lines were derived and characterized in our laboratory (Mateizel et al., 2006) and are registered in the EU hESC registry (https://hpscreg.eu/). hESC were cultured at 37°C in 5% CO_2 and atmospheric O_2 conditions, on 10 µg/ml laminin-521 (LN521; Biolamina) and in NutriStem® hESC XF medium (Biological Industries), supplemented with 100 U/ml penicillin/streptomycin (Pen/Strep; Thermo Fisher Scientific). Cell passaging was performed using 1x TrypLE™ Express (Thermo Fisher Scientific).

Skeletal myogenic progenitor differentiation of all hESCs lines was performed according to protocols described in van der Wal et al. (2017), with only few adjustments. Briefly, a total of 50,000 cells were plated on a 1.9 cm^2 dish, coated with 10 µg/ml laminin-521 (LN521; Biolamina). The next day, differentiation was induced by using 10 µM CHIR99021 (Axon MEDCHEM), in myogenic differentiation medium composed of DMEM-F12, 1x ITS-X, 100x Penicillin/Streptomycin/L-Glutamine (all from Thermo Fisher Scientific) (adapted from van der Wal et al. 2017) for 2 days. Subsequently, the CHIR99021 component in the myogenic differentiation medium was replaced by 20 ng/ml FGF2 (Prepotech) for the following 14 days. Myogenic differentiation medium without supplement was used for the last days of the 35 days during differentiation protocol. Medium was refreshed daily.

Following 35 days of differentiation, purification of myogenic progenitors from a mixed cell population was performed using FACS sorting as described in van der Wal et al. (2017). Briefly, cells were harvested with 1x TrypLE™ Express (Thermo Fisher Scientific) and filtered using a 40 µM FACS strainer. Subsequently, the cell suspension was incubated with the appropriate fluorochrome-labelled antibodies (Table S8) as mentioned by van der Wal et al. (2017). Labelled cells were sorted through a FACSAria (BD Biosciences) and collected in myogenic progenitor proliferation medium composed of DMEM high glucose, 10% fetal bovine serum, 100x Penicillin/Streptomycin/L-Glutamine, 1x RevitaCell supplement (all from Thermo Fisher Scientific) and 100 ng/ml FGF2 (Prepotech) (adopted from van der Wal et al. 2017). Captured cells were subsequently plated on a 10 µg/ml laminin-521 (LN521; Biolamina) coated 3.5 cm^2 dish and were cultured until confluency in myogenic progenitor proliferation medium without the 1x RevitaCell supplement.

When the sorted myogenic progenitors reach confluency, they can either be cryopreserved, expanded or differentiated towards multinucleated myotubes. The myogenic progenitor proliferation medium was continuously used after FACS sorting, supplemented with 10% DMSO for cryopreservation and replaced by myogenic differentiation medium without supplement for further differentiation towards multinucleated myotubes. Differentiation was started when progenitors reached confluency and harvested after 4 days of differentiation.

Neuroectoderm differentiation

The protocol for neuroectoderm was adapted from Chetty et al. (2013) and Chambers et al. (2009). hESC were passaged on laminin-521, as described above, 1–2 days prior to neuroectoderm differentiation in a ratio of 50,000–100,000 cells per cm^2 so that they were 90% confluent on the starting day. The neuroectoderm differentiation medium was refreshed daily and consisted of KnockOut™ DMEM (Thermo Fisher Scientific) with 10% KnockOut™ Serum Replacement (Thermo Fisher Scientific) and supplemented with 500 ng/ml Recombinant Human Noggin Protein (R&D Systems) and 10µM SB431542 (Tocris). Differentiated cells were collected after 12 days of differentiation.

DNA, RNA extraction and cDNA conversion

DNA was extracted using the DNAeasy Blood & Tissue kit and DNAeasy Micro kit (QIAGEN) and total RNA using the RNAeasy Mini kit (QIAGEN), following the manufacturers' guidelines. RNA was reverse-transcribed to cDNA using the First-Strand cDNA Synthesis Kit (GE Healthcare) following the manufacturers' guidelines.

qRT-PCR

Expression analysis on myogenic progenitor cells was performed using ViiA7 Real-Time PCR system (Thermo Fisher Scientific) and analysed with VIIA7 software v1.2 (Thermo Fisher Scientific). The 20 µl reaction mix contained 40 ng cDNA, 10 µl TaqMan® Fast Advanced Master Mix (Applied Biosystems) and either 1 µl TaqMan assay (Thermo Fisher Scientific) for *MYOG*, *MYOD1* or 1,8 µM primer mix (IDT) and 250 nM probes (Thermo Fisher Scientific) for *GAPDH* and *UBC* (Table S15). *GAPDH* and *UBC* were used as endogenous controls. Expression analysis on neuroectoderm was similar as above but was performed on 20 ng cDNA input and qPCR Mastermix Plus-low ROX (Eurogentec) was used. The TaqMan assay for *PAX6* was used and *GUSB* and *UBC* (Table S15) were the endogenous controls.

Immunocytochemistry

Skeletal muscle cells were fixed with 4% paraformaldehyde (PFA) for 10 min at room temperature, washed twice with PBS and permeabilized using 0.3% Triton-X (Sigma-Aldrich) for 10 min. The cells were blocked with PBS with 3% BSA and 0.1% Tween for 30 min, and were incubated with the primary for 1 h, in PBS with 0.1% BSA and 0.1% Tween. The secondary antibody was incubated for 30 min, in PBS with 0.1% BSA and 0.1% Tween. Images were taken by confocal microscopy using an LSM800 (Carl Zeiss). An estimation of the skeletal muscle differentiation efficiency was performed by calculating the ratio of the number of nuclei within a MF20 positive cell on the total amount of nuclei present. For neuroectoderm, the cells were permeabilized with 0.1% Triton (Sigma-Aldrich) and blocked with 10% Fetal Bovine Serum (Thermo Fisher Scientific). The antibodies were diluted in 3% BSA, 0.1% tween, 10% Fetal Bovine Serum in PBS. The primary antibody was incubated overnight at 4°C and the secondary antibody was incubated for 2–3 h at RT. The full list of antibodies and their dilutions can be found in the Table S16.

Analysis of CTG instability by PacBio Massive Parallel Sequencing

In order to amplify only one to five DNA molecules per reaction, we used a small pool PCR with an input of 20 to 50 pg as described in Seriola et al. (2011). For each cell DNA sample, 20 PCR reactions with low input template DNA were analysed to establish the distribution of the repeat sizes in each sample (De Temmerman et al., 2008; Seriola et al., 2011; Barbé et al., 2017). Repeats were amplified with high fidelity using the LongAmp Taq polymerase (New England Biolabs). Twenty to 50 pg of DNA was amplified in a 25 µl reaction mix containing 2.5 units LongAmp Taq DNA polymerase, 1x LongAmp buffer (New England Biolabs), 0.2 mM dNTPs (Illustra DNA polymerization mix, GE Healthcare) and 0.4 µM of primers DM101 and DM102 (Integrated DNA Technologies) (Brook et al., 1992) and 2.5% dimethyl sulfoxide (DMSO). Primer sequences are listed in Table S17. Amplification conditions were as follows: 4 min of initial denaturation at 94°C, 35 cycles of 30 s denaturation at 94°C, 8 min annealing and extension at 65°C and a final extension step at 65°C for 10 min. The LongAmp amplicons, spanning the repeat, were prepared for sequencing as described in PacBio's guide for Preparing SMRTbell™

Libraries using PacBio® Barcoded Adapters for Multiplex SMRT® Sequencing. This protocol allows to pool two samples in one library that each consist of 20 PCR products with a different barcode. Before exonuclease treatment, 500 ng of PUC19 plasmid was added to avoid degradation of intact SMRTbells. Each library was sequenced on a single SMRT cell by a PacBio RS II or Sequel using the DNA/Polymerase binding Kit P6 v2 (Pacific Biosciences) for a 360 min movie. We used PacBio's DNA Sequencing Reagent Kit 4.0 v2 for all runs. Therefore, demultiplexed circular consensus (CCS) reads were generated with the RS_ReadsOfInsert.1 protocol from PacBio's SMRT portal (v2.3.0) or with ccs and lima software from SMRTLink (v6.0.0) with a minimum of one full pass, a minimum predicted accuracy of 90% and demultiplexing with symmetric barcodes. Next, each PCR product was aligned to the *DMPK* CTG repeat using BWA-SW v0.7.10 (Li and Durbin, 2009) against the human reference genome hg19 downloaded from UCSC (Karolchik et al., 2004), followed by conversion of SAM to BAM by Samtools v1.3.1 (Li et al., 2009). To finally convert to BED format and select the on-target CCS reads BEDtools v2.20.1 was used (Quinlan and Hall, 2010). For each CCS read spanning the CTG repeat, the number of repeat units was determined by measuring the distance between two unique regions flanking the CTG repeat followed by detecting the most abundantly present repeat size in each PCR product, here represented by the median.

Bisulfite treatment and massive parallel sequencing

Bisulfite treated massive parallel sequencing was performed as described by Barbé et al. (2017). Briefly, the Imprint DNA Modification Kit (Sigma-Aldrich) was used for bisulfite treatment on 200 ng DNA. Bisulfite-treated DNA was amplified using primers in Table S17 for regions upstream (CTCF1) and downstream (CTCF2) of the CTG repeat, using the Jumpstart Taq DNA Polymerase Kit (Sigma-Aldrich). The first and second round PCR conditions were adapted from Barbé et al. (2017). First round PCR primers (Table S17) are indicated by '1' at the end of the target name, second round primers (Table S17) are indicated by Miseq at the end of the target name. Libraries were made as described in Barbé et al. (2017) and subsequently loaded on the MiSeq Reagent Nano Kit v2 (500 cycles) according to the manufacturer's instructions and sequenced at 2×250 bp (Illumina). During data analysis, we used on online tool (https://tabsat.ait.ac.at) that includes all sequences that have been sequenced.

RNA sequencing and analysis

Total RNA was quality checked using a Fragment Analyzer, and 500 ng was depleted of rRNA (NEBNext rRNA Depletion kit, NEB) and cDNA libraries prepared (NEBNext UltraII Directional RNA library prep kit, NEB). Sequencing was performed on the NextSeq500 Illumina platform using version 2.5 chemistry. Fastq files were inspected using FastQC [FastQC: A Quality Control Tool for High Throughput Sequence Data: http://www.bioinformatics.babraham.ac.uk/projects/fastqc/ (2015)]. Reads were filtered and trimmed to a read length of 70 using BBDuk (sourceforge.net/projects/bbmap). For the RNAseq analysis, Fastq sequences were mapped against the Genome Reference Consortium Human Build 38 (GRCh38.p13). The software used for mapping was STAR (version 2.7.3) (Dobin et al., 2013). The RNA-seq by Expectation Maximization (RSEM) (Li and Dewey, 2011) software (version 1.3.2) was used to produce the count table for each sample. RSEM algorithm was chosen because it is optimized for multi-mapped reads. The RNA-seq analysis was performed using the R software (version 3.6.3) with the edgeR (Robinson et al., 2009) and DESeq2 (Love et al., 2014) libraries. Only genes with a count per million (cpm) greater than 1 in at least two samples were considered. The raw counts were normalized using the trimmed mean of M values (Robinson and Oshlack, 2010) (TMM) algorithm. For each comparison, a different general linear model was built. Statistical testing was done using the empirical Bayes quasi-likelihood *F*-test. The normalized counts were then transformed in a $\log_2$ fold-change ($\log_2$FC) table with their associated statistics, *P*-value and false discovery rate (FDR). In each comparison, genes with a $|\log_2 FC|>1$ and an FDR<0.05 were considered as significantly differentially expressed. A $|\log_2 FC|>1$ means at least two times more or two times less transcript in the test group in comparison to the control group. The Gene set enrichment analysis (GSEA) software was downloaded from (http://software.broadinstitute.org/gsea/). The ranking score for each score was computed for each coding gene CPM>1 in at least two samples. The parameters set for each analysis were: enrichment statistic as weighted, number of permutations was 1000, exclude sets larger than 500 and exclude sets smaller than 15. The libraries used from Molecular Signatures Database v6.2 (MSigDB) were hallmark gene sets (H), curated gene sets (C2) and ontology gene sets (C5). The gene sets were statistically relevant if their FDR was below 0.05. The gene sets were considered as positively enriched if their normalized enriched score (NES) was above 1.4 and negatively enriched if their NES<−1.4 (Subramanian et al., 2005).

For splicing analysis, files were aligned to the human genome (hg38) using STAR (v2.6.0a) (Dobin et al., 2013) and splicing was quantified using rMATS (v4.0.2) (Shen et al., 2014). All splicing events were categorised in five different classes of splicing events: cassette or skipped exon (SE), mutually exclusive exon (MXE), alternative 5′ splice site (A5SS), alternative 3′ splice site (A3SS) and retained intron (RI) events. Data were filtered based on average read number ≥5 and FDR ≤0.05 and the percentage spliced-in (Ψ, PSI) was calculated. This dataset was further used to compare non-DM1 with DM1 samples using the change in percent spliced in ($\Delta\Psi$) and splicing events with a cut-off of $|\Delta\Psi|>0.1$ were further included. We also analysed splicing events over the timecourse of myogenic differentiation based on average read number ≥5 and FDR ≤0.05 and cut-off of $|\Delta\Psi|>0.1$.

Statistics

We used the Jonckheere-Terpstra Test, which is based on comparing medians to study differences in median repeat size across cell lines and conditions. A result of $P<0.05$ in the Jonckheere-Terpstra test indicates that our data follows a specific trend.

Acknowledgements

We thank Prof. Dr. Pim Pijnappel and his lab for their help with the skeletal muscle differentiation. We acknowledge the technical support by the team of BRIGHTCore for the Miseq analysis. We also acknowledge the Genomics Core at UZ Leuven for their technical support for PacBio sequencing.

Competing interests

The authors declare no competing or financial interests.

Author contributions

Conceptualization: A.G., C.S., K.D.S.; Methodology: S.F., J.L.B., C.M., L.B., J.A., P.H., G.D., M.S.S.; Software: E.C.D.D., J.L.B., C.S.; Formal analysis: S.F., E.C.D.D., C.M., L.B., J.A., P.H., G.D., C.S.; Resources: K.D.S.; Data curation: S.F., E.C.D.D., J.L.B., C.S.; Writing - original draft: S.F., J.L.B., A.G., K.D.S.; Writing - review & editing: E.C.D.D., C.M., L.B., J.A., M.S.S., C.S., K.D.S.; Visualization: S.F.; Supervision: M.S.S., A.G., C.S., K.D.S.; Project administration: K.D.S.; Funding acquisition: K.D.S.

Funding

This work was supported by the Methusalem grant in name of Karen Sermon, Fonds voor Wetenschappelijk Onderzoek Vlaanderen (FWO) (G.0223.15N) and by the Hercules foundation (ZW11-14).

Data availability

The datasets produced in this study are available in the following databases: RNA-Seq data: GEO database number: GSE160916 (https://www.ncbi.nlm.nih.gov/geo/query/acc.cgi?acc=GSE160916).

References

Barbé, L., Lanni, S., López-Castel, A., Franck, S., Spits, C., Keymolen, K., Seneca, S., Tomé, S., Miron, I., Letourneau, J. et al. (2017). CpG methylation, a parent-of-origin effect for maternal-biased transmission of congenital myotonic dystrophy. *Am. J. Hum. Genet.* **100**, 488-505. doi:10.1016/j.ajhg.2017.01.033

Beffy, P., del Carratore, R., Masini, M., Furling, D., Puymirat, J., Masiello, P. and Simili, M. (2010). Altered signal transduction pathways and induction of autophagy in human myotonic dystrophy type 1 myoblasts. *Int. J. Biochem. Cell Biol.* **42**, 1973-1983. doi:10.1016/j.biocel.2010.08.010

Bouchard, J.-P., Cossette, L., Bassez, G. and Puymirat, J. (2015). Natural history of skeletal muscle involvement in myotonic dystrophy type 1: a retrospective study in 204 cases. *J. Neurol.* **262**, 285-293. doi:10.1007/s00415-014-7570-x

Brinegar, A. E., Xia, Z., Loehr, J. A., Li, W., Rodney, G. G. and Cooper, T. A. (2017). Extensive alternative splicing transitions during postnatal skeletal muscle

development are required for calcium handling functions. *eLife* **6**, e27192. doi:10.7554/eLife.27192

Brockhoff, M., Rion, N., Chojnowska, K., Wiktorowicz, T., Eickhorst, C., Erne, B., Frank, S., Angelini, C., Furling, D., Rüegg, M. A. et al. (2017). Targeting deregulated AMPK/mTORC1 pathways improves muscle function in myotonic dystrophy type i. *J. Clin. Investig.* **127**:549-563. doi:10.1172/JCI89616

Brook, J. D. D., McCurrach, M. E., Harley, H. G., Buckler, A. J., Church, D., Aburatani, H., Hunter, K., Stanton, V. P., Thirion, J.-P. P., Hudson, T. et al. (1992). Molecular basis of myotonic dystrophy: expansion of a trinucleotide (CTG) repeat at the 3′ end of a transcript encoding a protein kinase family member. *Cell* **68**, 799-808. doi:10.1016/0092-8674(92)90154-5

Brouwer, J. R., Huguet, A., Nicole, A., Munnich, A. and Gourdon, G. (2013). Transcriptionally repressive chromatin remodelling and CpG methylation in the presence of expanded CTG-repeats at the DM1 Locus. *J. Nucleic Acids* **2013**, 567435. doi:10.1155/2013/567435

Carrell, S. T., Carrell, E. M., Auerbach, D., Pandey, S. K., Bennett, C. F., Dirksen, R. T. and Thornton, C. A. (2016). Dmpk gene deletion or antisense knockdown does not compromise cardiac or skeletal muscle function in mice. *Hum. Mol. Genet.* **25**, 4328-4338. doi:10.1093/hmg/ddw266

Chambers, S. M., Fasano, C. A., Papapetrou, E. P., Tomishima, M., Sadelain, M. and Studer, L. (2009). Highly efficient neural conversion of human ES and iPS cells by dual inhibition of SMAD signaling. *Nat. Biotechnol.* **27**, 275-280. doi:10.1038/nbt.1529

Chetty, S., Pagliuca, F. W., Honore, C., Kweudjeu, A., Rezania, A. and Melton, D. A. (2013). A simple tool to improve pluripotent stem cell differentiation. *Nat. Methods* **10**, 553-556. doi:10.1038/nmeth.2442

Cowling, B. S., Prokic, I., Tasfaout, H., Rabai, A., Humbert, F., Rinaldi, B., Nicot, A.-S., Kretz, C., Friant, S., Roux, A. et al. (2017). Amphiphysin (BIN1) negatively regulates dynamin 2 for normal muscle maturation. *J. Clin. Invest.* **127**, 4477-4487. doi:10.1172/JCI90542

De Antonio, M., Dogan, C., Hamroun, D., Mati, M., Zerrouki, S., Eymard, B., Katsahian, S. and Bassez, G. (2016). Unravelling the myotonic dystrophy type 1 clinical spectrum: A systematic registry-based study with implications for disease classification. *Rev. Neurol. (Paris)* **172**, 572-580. doi:10.1016/j.neurol.2016.08.003

De Temmerman, N., Seneca, S., Van Steirteghem, A., Haentjens, P., Van der Elst, J., Liebaers, I. and Sermon, K. D. (2008). CTG repeat instability in a human embryonic stem cell line carrying the myotonic dystrophy type 1 mutation. *Mol. Hum. Reprod.* **14**, 405-412. doi:10.1093/molehr/gan034

Denis, J. A., Gauthier, M., Rachdi, L., Aubert, S., Giraud-Triboult, K., Poydenot, P., Benchoua, A., Champon, B., Maury, Y., Baldeschi, C. et al. (2013). mTOR-dependent proliferation defect in human ES-derived neural stem cells affected by myotonic dystrophy type 1. *J. Cell Sci.* **126**, 1763-1772. doi:10.1242/jcs.116285

Dobin, A., Davis, C. A., Schlesinger, F., Drenkow, J., Zaleski, C., Jha, S., Batut, P., Chaisson, M. and Gingeras, T. R. (2013). STAR: ultrafast universal RNA-seq aligner. *Bioinformatics* **29**, 15-21. doi:10.1093/bioinformatics/bts635

Dort, J., Fabre, P., Molina, T. and Dumont, N. A. (2019). Macrophages are key regulators of stem cells during skeletal muscle regeneration and diseases. *Stem Cells Int.* **2019**, 4761427. doi:10.1155/2019/4761427

Eriksson, M., Hedberg, B., Carey, N. and Ansved, T. (2001). Decreased DMPK transcript levels in myotonic dystrophy 1 type IIA muscle fibers. *Biochem. Biophys. Res. Commun.* **286**, 1177-1182. doi:10.1006/bbrc.2001.5516

Farkas-Bargeton, E., Barbet, J. P., Dancea, S., Wehrle, R., Checouri, A. and Dulac, O. (1988). Immaturity of muscle fibers in the congenital form of myotonic dystrophy: Its consequences and its origin. *J. Neurol. Sci.* **83**, 145-159. doi:10.1016/0022-510X(88)90064-0

Fugier, C., Klein, A. F., Hammer, C., Vassilopoulos, S., Ivarsson, Y., Toussaint, A., Tosch, V., Vignaud, A., Ferry, A., Messaddeq, N. et al. (2011). Misregulated alternative splicing of BIN1 is associated with T tubule alterations and muscle weakness in myotonic dystrophy. *Nat. Med.* **17**, 720-725. doi:10.1038/nm.2374

Furling, D., Lemieux, D., Taneja, K. and Puymirat, J. (2001a). Decreased levels of myotonic dystrophy protein kinase (DMPK) and delayed differentiation in human myotonic dystrophy myoblasts. *Neuromuscul. Disord.* **11**, 728-735. doi:10.1016/S0960-8966(01)00226-7

Furling, D., Coiffier, L., Mouly, V., Barbet, J. P., St Guily, J. L., Taneja, K., Gourdon, G., Junien, C. and Butler-Browne, G. S. (2001b). Defective satellite cells in congenital myotonic dystrophy. *Hum. Mol. Genet.* **10**, 2079-2087. doi:10.1093/hmg/10.19.2079

Jenquin, J. R., Yang, H., Huigens, R. W., III, Nakamori, M. and Berglund, J. A. (2019). Combination treatment of erythromycin and furamidine provides additive and synergistic rescue of Mis-splicing in myotonic dystrophy type 1 models. *ACS Pharmacol. Transl. Sci.* **2**, 247-263. doi:10.1021/acsptsci.9b00020

Johnson, N. E., Butterfield, R., Berggren, K., Hung, M., Chen, W., Dibella, D., Dixon, M., Hayes, H., Pucillo, E., Bounsanga, J. et al. (2016). Disease burden and functional outcomes in congenital myotonic dystrophy: A cross-sectional study. *Neurology* **87**, 160-167. doi:10.1212/WNL.0000000000002845

Karolchik, D., Hinrichs, A. S., Furey, T. S., Roskin, K. M., Sugnet, C. W., Haussler, D. and Kent, W. J. (2004). The UCSC Table Browser data retrieval tool. *Nucleic Acids Res.* **32**, 493-496. doi:10.1093/nar/gkh103

Koebis, M., Ohsawa, N., Kino, Y., Sasagawa, N., Nishino, I. and Ishiura, S. (2011). Alternative splicing of myomesin 1 gene is aberrantly regulated in myotonic dystrophy type 1. *Genes Cells* **16**, 961-972. doi:10.1111/j.1365-2443.2011.01542.x

Li, B. and Dewey, C. N. (2011). RSEM: accurate transcript quantification from RNA-Seq data with or without a reference genome. *BMC Bioinformatics* **12**, 323. doi:10.1186/1471-2105-12-323

Li, H. and Durbin, R. (2009). Fast and accurate short read alignment with Burrows-Wheeler transform. *Bioinformatics* **25**, 1754-1760. doi:10.1093/bioinformatics/btp324

Li, H., Handsaker, B., Wysoker, A., Fennell, T., Ruan, J., Homer, N., Marth, G., Abecasis, G. and Durbin, R. (2009). The Sequence Alignment/Map format and SAMtools. *Bioinformatics* **25**, 2078-2079. doi:10.1093/bioinformatics/btp352

López Castel, A., Nakamori, M., Tomé, S., Chitayat, D., Gourdon, G., Thornton, C. A. and Pearson, C. E. (2011). Expanded CTG repeat demarcates a boundary for abnormal CpG methylation in myotonic dystrophy patient tissues. *Hum. Mol. Genet.* **20**, 1-15. doi:10.1093/hmg/ddq427

Loro, E., Rinaldi, F., Malena, A., Masiero, E., Novelli, G., Angelini, C., Romeo, V., Sandri, M., Botta, A. and Vergani, L. (2010). Normal myogenesis and increased apoptosis in myotonic dystrophy type-1 muscle cells. *Cell Death Differ.* **17**, 1315-1324. doi:10.1038/cdd.2010.33

Love, M. I., Huber, W. and Anders, S. (2014). Moderated estimation of fold change and dispersion for RNA-seq data with DESeq2. *Genome Biol.* **15**, 550. doi:10.1186/s13059-014-0550-8

Mahadevan, M., Tsilfidis, C., Sabourin, L., Shutler, G., Amemiya, C., Jansen, G., Neville, C., Narang, M., Barceló, J., O'Hoy, K. et al. (1992). Myotonic dystrophy mutation: an unstable CTG repeat in the 3′ untranslated region of the gene. *Science* **255**, 1253-1255. doi:10.1126/science.1546325

Martorell, L., Johnson, K., Boucher, C. A. and Baiget, M. (1997). Somatic instability of the myotonic dystrophy (CTG)n repeat during human fetal development. *Hum. Mol. Genet.* **6**, 877-880. doi:10.1093/hmg/6.6.877

Masuda, A., Andersen, H. S., Doktor, T. K., Okamoto, T., Ito, M., Andresen, B. S. and Ohno, K. (2012). CUGBP1 and MBNL1 preferentially bind to 3′ UTRs and facilitate mRNA decay. *Sci. Rep.* **2**, 209. doi:10.1038/srep00209

Mateizel, I., De Temmerman, N., Ullmann, U., Cauffman, G., Sermon, K., Van de Velde, H., De Rycke, M., Degreef, E., Devroey, P., Liebaers, I. et al. (2006). Derivation of human embryonic stem cell lines from embryos obtained after IVF and after PGD for monogenic disorders. *Hum. Reprod.* **21**, 503-511. doi:10.1093/humrep/dei345

Nakamori, M., Hamanaka, K., Thomas, J. D., Wang, E. T., Hayashi, Y. K., Takahashi, M. P., Swanson, M. S., Nishino, I. and Mochizuki, H. (2017). Aberrant myokine signaling in congenital myotonic dystrophy. *Cell Rep.* **21**, 1240-1252. doi:10.1016/j.celrep.2017.10.018

Nutter, C. A., Bubenik, J. L., Oliveira, R., Ivankovic, F., Sznajder, Ł. J., Kidd, B. M., Pinto, B. S., Otero, B. A., Carter, H. A., Vitriol, E. A. et al. (2019). Cell-type-specific dysregulation of RNA alternative splicing in short tandem repeat mouse knockin models of myotonic dystrophy. *Genes Dev.* **33**, 1635-1640. doi:10.1101/gad.328963.119

Otis, J. S., Niccoli, S., Hawdon, N., Sarvas, J. L., Frye, M. A., Chicco, A. J. and Lees, S. J. (2014). Pro-inflammatory mediation of myoblast proliferation. *PLoS ONE* **9**, e92363. doi:10.1371/journal.pone.0092363

Pistoni, M., Ghigna, C. and Gabellini, D. (2010). Alternative splicing and muscular dystrophy. *RNA Biol.* **7**, 441-452. doi:10.4161/rna.7.4.12258

Prokic, I., Cowling, B. S., Kutchukian, C., Kretz, C., Tasfaout, H., Gache, V., Hergueux, J., Wendling, O., Ferry, A., Toussaint, A. et al. (2020). Differential physiological roles for BIN1 isoforms in skeletal muscle development, function and regeneration. *Dis. Model Mech.* **13**, 1-15. doi:10.1242/dmm.044354.

Provenzano, C., Cappella, M., Valaperta, R., Cardani, R., Meola, G., Martelli, F., Cardinali, B. and Falcone, G. (2017). CRISPR/Cas9-mediated deletion of CTG expansions recovers normal phenotype in myogenic cells derived from myotonic dystrophy 1 patients. *Mol. Ther. Nucleic Acids* **9**, 337-348. doi:10.1016/j.omtn.2017.10.006

Quinlan, A. R. and Hall, I. M. (2010). BEDTools: A flexible suite of utilities for comparing genomic features. *Bioinformatics* **26**, 841-842. doi:10.1093/bioinformatics/btq033

Rion, N., Castets, P., Lin, S., Enderle, L., Reinhard, J. R., Eickhorst, C. and Ruegg, M. A. (2019). MTOR controls embryonic and adult myogenesis via mTORC1. *Development* **146**, dev172460. doi:10.1242/dev.172460

Rizzo, M., Beffy, P., Del Carratore, R., Falleni, A., Pretini, V., D'Aurizio, R., Botta, A., Evangelista, M., Stoccoro, A., Coppedè, F. et al. (2018). Activation of the interferon type I response rather than autophagy contributes to myogenesis inhibition in congenital DM1 myoblasts. *Cell Death Dis.* **9**, 1-16. doi:10.1038/s41419-018-1080-1

Robinson, M. D. and Oshlack, A. (2010). A scaling normalization method for differential expression analysis of RNA-seq data. *Genome Biol.* **11**, R25. doi:10.1186/gb-2010-11-3-r25

Robinson, M. D., McCarthy, D. J. and Smyth, G. K. (2009). edgeR: a Bioconductor package for differential expression analysis of digital gene expression data. *Bioinformatics* **26**, 139-140. doi:10.1093/bioinformatics/btp616

Salvatori, S., Fanin, M., Trevisan, C. P., Furlan, S., Reddy, S., Nagy, J. I. and Angelini, C. (2005). Decreased expression of DMPK: Correlation with CTG repeat expansion and fibre type composition in myotonic dystrophy type 1. *Neurol. Sci.* **26**, 235-242. doi:10.1007/s10072-005-0466-x

Sarnat, H. B. (2011). Maturational arrest of fetal muscle in neonatal myotonic dystrophy. *Arch. Neurol.* **33**, 466. doi:10.1001/archneur.1976.00500070008002

Seriola, A., Spits, C., Simard, J. P., Hilven, P., Haentjens, P., Pearson, C. E. and Sermon, K. (2011). Huntington's and myotonic dystrophy hESCs: down-regulated trinucleotide repeat instability and mismatch repair machinery expression upon differentiation. *Hum. Mol. Genet.* **20**, 176-185. doi:10.1093/hmg/ddq456

Shen, S., Park, J. W., Lu, Z.-X., Lin, L., Henry, M. D., Wu, Y. N., Zhou, Q. and Xing, Y. (2014). rMATS: Robust and flexible detection of differential alternative splicing from replicate RNA-Seq data. *Proc. Natl. Acad. Sci. USA* **111**, E5593-E5601. doi:10.1073/pnas.1419161111

Subramanian, A., Tamayo, P., Mootha, V. K., Mukherjee, S., Ebert, B. L., Gillette, M. A., Paulovich, A., Pomeroy, S. L., Golub, T. R., Lander, E. S. et al. (2005). Gene set enrichment analysis: A knowledge-based approach for interpreting genome-wide expression profiles. *Proc. Natl. Acad. Sci. USA* **102**, 15545-15550. doi:10.1073/pnas.0506580102

Thomas, J. D., Sznajder, Ł. J., Bardhi, O., Aslam, F. N., Anastasiadis, Z. P., Scotti, M. M., Nishino, I., Nakamori, M., Wang, E. T. and Swanson, M. S. (2017). Disrupted prenatal RNA processing and myogenesis in congenital myotonic dystrophy. *Genes Dev.* **31**, 1122-1133. doi:10.1101/gad.300590.117

Udd, B. and Krahe, R. (2012). The myotonic dystrophies: Molecular, clinical, and therapeutic challenges. *Lancet Neurol.* **11**, 891-905. doi:10.1016/S1474-4422(12)70204-1

van Agtmaal, E. L., André, L. M., Willemse, M., Cumming, S. A., van Kessel, I. D. G., van den Broek, W. J. A. A., Gourdon, G., Furling, D., Mouly, V., Monckton, D. G. et al. (2017). CRISPR/Cas9-induced (CTG·CAG)n repeat instability in the myotonic dystrophy type 1 locus: implications for therapeutic genome editing. *Mol. Ther.* **25**, 24-43. doi:10.1016/j.ymthe.2016.10.014

van der Wal, E., Bergsma, A. J., van Gestel, T. J. M., in 't Groen, S. L. M., Zaehres, H., Araúzo-Bravo, M. J., Schöler, H. R., van der Ploeg, A. T. and Pijnappel, W. W. M. P. (2017). GAA deficiency in pompe disease is alleviated by exon inclusion in iPSC-derived skeletal muscle cells. *Mol. Ther. Nucleic Acids* **7**, 101-115. doi:10.1016/j.omtn.2017.03.002

Wagner, S. D., Struck, A. J., Gupta, R., Farnsworth, D. R., Mahady, A. E., Eichinger, K., Thornton, C. A., Wang, E. T. and Berglund, J. A. (2016). Dose-dependent regulation of alternative splicing by MBNL proteins reveals biomarkers for myotonic dystrophy. *PLoS Genet.* **12**, 1-24. doi:10.1371/journal.pgen.1006316

Wang, E. T., Cody, N. A. L., Jog, S., Biancolella, M., Wang, T. T., Treacy, D. J., Luo, S., Schroth, G. P., Housman, D. E., Reddy, S. et al. (2012). Transcriptome-wide regulation of pre-mRNA splicing and mRNA localization by muscleblind proteins. *Cell* **150**, 710-724. doi:10.1016/j.cell.2012.06.041

Wang, Y., Hao, L., Li, H., Cleary, J. D., Tomac, M. P., Thapa, A., Guo, X., Zeng, D., Wang, H., McRae, M. K. et al. (2019). Abnormal nuclear aggregation and myotube degeneration in myotonic dystrophy type 1. *Neurol. Sci.* **40**, 1255-1265. doi:10.1007/s10072-019-03783-w

Yanovsky-Dagan, S., Avitzour, M., Altarescu, G., Renbaum, P., Eldar-Geva, T., Schonberger, O., Mitrani-Rosenbaum, S., Levy-Lahad, E., Birnbaum, R. Y., Gepstein, L. et al. (2015). Uncovering the role of hypermethylation by CTG expansion in myotonic dystrophy type 1 using mutant human embryonic stem cells. *Stem Cell Rep.* **5**, 221-231. doi:10.1016/j.stemcr.2015.06.003

Supplemental data

Table of contents

FIG. S1: CTG REPEAT SIZE IN THE FOUR HESCS AND THEIR DERIVED MYOBLASTS AND MYOTUBES. 2

TABLE S1: INDIVIDUAL CTG REPEAT VALUES FOR THE FIG. S1 AND IS PRESENTED IN A SEPARATE EXCEL SHEET. 3

FIG. S2: SAMPLES CLUSTER TOGETHER ACCORDING TO CELL TYPE NOT ACCORDING TO DM1 VS NON-DM1. ..4

TABLE S2: LIST OF GO PATHWAYS RELATED TO MUSCLE DIFFERENTIATION COMMONLY OR DIFFERENTIALLY REGULATED IN DM1 OR NON-DM1 CELL LINES FROM HUMAN EMBRYONIC STEM CELLS TO MYOBLASTS. 5

TABLE S3: LIST OF GO PATHWAYS RELATED TO MUSCLE DIFFERENTIATION COMMONLY OR DIFFERENTIALLY REGULATED IN DM1 OR NON-DM1 CELL LINES FROM MYOBLASTS TO MYOTUBES. 7

TABLE S4: GENES INCLUDED IN THE HEATMAP IN FIGURE 1E. 9

TABLE S5: GENES INCLUDED IN THE HEATMAP IN FIGURE 2D. 12

FIG. S3. HEATMAPS REPRESENTING THE LOG FOLD CHANGE OF GENES BELONGING TO IL6 JAK STAT3 SIGNALING, AND TNFA SIGNALING VIA NFKB PATHWAYS. 15

TABLE S6: GENES INCLUDED IN THE HEATMAPS IN FIGURE 3B AND FIG. S3. 16

FIG. S4: THE CPG METHYLATION DOWNSTREAM OF THE CTG REPEAT IN DM1 SAMPLES AND NON-DM1 SAMPLES OVER THE COURSE OF DIFFERENTIATION. 31

FIG. S5: CHARACTERIZATION OF THE CELLS AFTER NEUROECTODERM DIFFERENTIATION. 32

FIG. S6: THE UPSTREAM CPG METHYLATION TENDS TO INCREASE OVER NEUROECTODERM DIFFERENTIATION IN DM1 SAMPLES, THE DOWNSTREAM CPG REGION REMAINS UNCHANGED. 33

TABLE S7: SPLICING DEFECTS COMPARING DM1 MYOBLASTS VERSUS MYOTUBES 34

TABLE S8: SPLICING DEFECTS COMPARING DM1 STEM CELLS VERSUS MYOTUBES 34

TABLE S9: SPLICING DEFECTS COMPARING NON-DM1 LINES VERSUS VUB03_DM1 34

TABLE S10: SPLICING DEFECTS COMPARING NON-DM1 MYOTUBES VERSUS DM1 MYOTUBES 34

TABLE S11: SPLICING COMPARING NON-DM1 MYOTUBES VERSUS NON-DM1 MYOTUBES 34

TABLE S12: SPLICING DEFECTS COMPARING NON-DM1 MYOTUBES VERSUS DM1 MYOTUBES 34

TABLE S13: SPLICING DEFECTS COMPARING NON-DM1 STEM CELLS VERSUS DM1 STEM CELLS 34

TABLE S14: SPLICING COMPARING NON-DM1 STEM CELLS VERSUS NON-DM1 MYOTUBES 34

TABLE S15: PROBES, ASSAYS AND PRIMERS FOR QRT-PCR. 34

TABLE S16: LIST OF USED ANTIBODIES AND MANUFACTURERS. 35

TABLE S17: LIST OF PRIMERS. 35

A

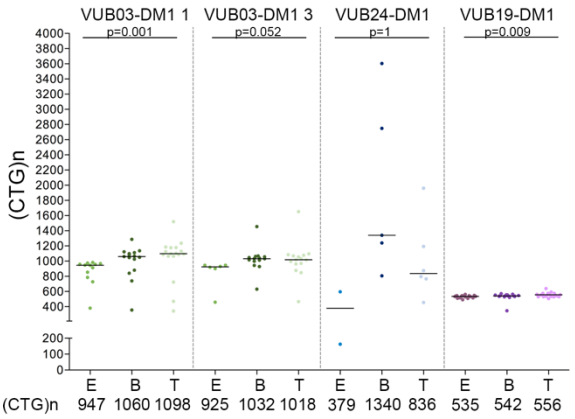

B

Jonckheere-Terpstra Test

VUB03-DM1 1 SC-MB-MT	data	VUB03-DM1 3 SC-MB-MT	data
number of levels	3	number of levels	3
N	43	N	35
Observed J-T Statistic	453	Observed J-T Statistic	255
Mean J-T statistic	303.5	Mean J-T statistic	192
std deviation of J-T statistic	44.631	std deviation of J-T statistic	32.357
std J-T statistic	3.35	std J-T statistic	1.95
Asymp. Sig. (2-tailed)	0.001	Asymp. Sig. (2-tailed)	0.052

VUB24-DM1 SC-MB-MT	data	VUB19-DM1 SC-MB-MT	data
number of levels	3	number of levels	3
N	13	N	54
Observed J-T Statistic	26	Observed J-T Statistic	649
Mean J-T statistic	26	Mean J-T statistic	485.5
std deviation of J-T statistic	7.461	std deviation of J-T statistic	62.97
std J-T statistic	0	std J-T statistic	2.596
Asymp. Sig. (2-tailed)	1	Asymp. Sig. (2-tailed)	0.009

Fig. S1. CTG repeat size in the four hESCs and their derived myoblasts and myotubes.

(A) The median CTG repeat size is shown for all 3 cell types (hESCs, myoblasts, myotubes) of VUB03-DM1, VUB24-DM1 and VUB19-DM1. Every dot represents the median repeat size of one low input LongAmp PCR reaction, and reflects the repeat size which was dominantly present in that PCR reaction. The horizontal line for every dot cluster represent the median for that cluster. Individual repeat sizes of every dot are presented in **Table S1**. **(B)** The Jonkheere-Terpstra test details. The Jonckheere-Terpstra test was performed on every hESC line separately, including the three different cell types. N is the number of data points.

Abbreviations: E and SC: human embryonic stem cells; B and MB: myoblasts; T and MT: myotubes.

Table S1. Individual CTG repeat values for the Fig. S1 and is presented in a separate excel sheet.

PacBio results are shown per individual LongAmp PCR reaction and per DM1 cell line for hESCs, myoblasts and myotubes. Number of reads, maximum and minimum repeat size, median and mean CTG repeat sizes are shown per PCR reaction. The values at the bottom of the rows with the mean and median per PCR reaction indicate the mean or median for the whole sample.

https://figshare.com/s/491658bfa49266b27e9a

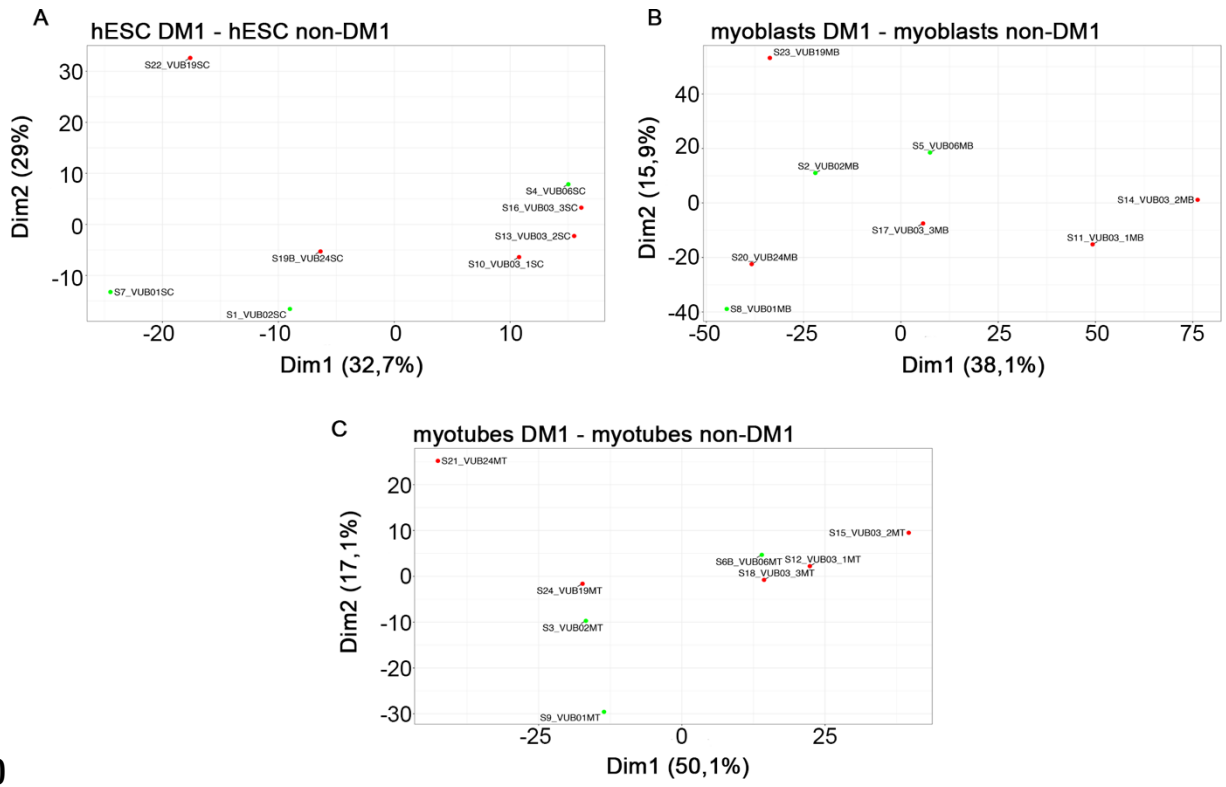

(A)

Fig. S2. Samples cluster together according to cell type not according to DM1 vs non-DM1.

(A) Principle component analysis of DM1 hESCs versus non-DM1 hESCs, **(B)** Principle component analysis of DM1 myoblasts versus non-DM1 myoblasts, **(C)** Principle component analysis of DM1 myotubes versus non-DM1 myotubes. Abbreviations: SC: human embryonic stem cells; MB: myoblasts; MT: myotubes.

Table S2. List of GO pathways related to muscle differentiation commonly or differentially regulated in DM1 or non-DM1 cell lines from human embryonic stem cells to myoblasts.

Abbreviations: NES: normalized enrichment score

common in DM1 and nonDM1		
pathway	**padj**	**NES**
GO_ACTIN_FILAMENT_BASED_PROCESS	0.01265662	1.82755139
GO_ACTIN_FILAMENT_BINDING	0.01265662	1.65965972
GO_ACTIN_FILAMENT_BUNDLE	0.01265662	1.72006638
GO_ACTIN_FILAMENT_ORGANIZATION	0.01265662	1.80606287
GO_ACTIN_MONOMER_BINDING	0.01265662	1.92364276
GO_ACTOMYOSIN	0.01265662	1.92669322
GO_MESODERM_DEVELOPMENT	0.02718075	1.51100596
GO_MESODERM_MORPHOGENESIS	0.01265662	2.09475924
GO_MESODERMAL_CELL_DIFFERENTIATION	0.02718075	1.79060856
GO_MUSCLE_CELL_DEVELOPMENT	0.03352309	1.53029422
GO_MUSCLE_CELL_DIFFERENTIATION	0.01265662	2.00327926
GO_MUSCLE_CELL_MIGRATION	0.01265662	2.0880279
GO_MUSCLE_STRUCTURE_DEVELOPMENT	0.01265662	2.14812435
GO_MUSCLE_TISSUE_DEVELOPMENT	0.01265662	2.11831806
GO_MYOBLAST_DIFFERENTIATION	0.01265662	1.91262265
GO_MYOBLAST_FUSION	0.01265662	1.97777147
GO_POSITIVE_REGULATION_OF_MUSCLE_ CELL_DIFFERENTIATION	0.01265662	1.88645592
GO_POSITIVE_REGULATION_OF_MYOBLAST_ DIFFERENTIATION	0.01265662	1.95881106
GO_POSITIVE_REGULATION_OF_MYOTUBE_ DIFFERENTIATION	0.02718075	1.70879793
GO_POSITIVE_REGULATION_OF_SKELETAL_ MUSCLE_TISSUE_DEVELOPMENT	0.02047867	1.74902239
GO_POSITIVE_REGULATION_OF_SMOOTH_MUSCLE_ CELL_MIGRATION	0.01265662	1.9709965
GO_POSITIVE_REGULATION_OF_STRIATED_MUSCLE_CELL_ DIFFERENTIATION	0.01265662	1.75918725
GO_REGULATION_OF_ACTIN_FILAMENT_BASED_ PROCESS	0.01265662	1.71984935

GO_REGULATION_OF_ACTIN_FILAMENT_DEPOLYMERIZATION	0.01265662	1.76999533
GO_REGULATION_OF_ACTIN_FILAMENT_LENGTH	0.01265662	1.87975112
GO_REGULATION_OF_MYOBLAST_DIFFERENTIATION	0.01265662	1.96570676
GO_REGULATION_OF_SKELETAL_MUSCLE_TISSUE_ DEVELOPMENT	0.01265662	1.92787985
GO_REGULATION_OF_SMOOTH_MUSCLE_CELL_ PROLIFERATION	0.01265662	1.64533319
GO_SKELETAL_MUSCLE_CELL_DIFFERENTIATION	0.01265662	1.8912858
GO_SKELETAL_MUSCLE_ORGAN_DEVELOPMENT	0.01265662	1.85674546
GO_SMOOTH_MUSCLE_CELL_DIFFERENTIATION	0.02047867	1.72172324
GO_SMOOTH_MUSCLE_TISSUE_DEVELOPMENT	0.01265662	2.10317899
only in nonDM1		
pathway	**padj**	**NES**
GO_MUSCLE_ORGAN_MORPHOGENESIS	0.02063181	1.79042048
GO_RESPONSE_TO_MUSCLE_STRETCH	0.0271632	1.72427596
GO_NEGATIVE_REGULATION_OF_MUSCLE_TISSUE_ DEVELOPMENT	0.0391335	1.6233145
GO_POSITIVE_REGULATION_OF_MUSCLE_TISSUE_ DEVELOPMENT	0.0391335	1.60740162
only in DM1		
pathway	**padj**	**NES**
GO_MUSCLE_CELL_PROLIFERATION	0.01265662	1.9935163
GO_MUSCLE_CELL_CELLULAR_HOMEOSTASIS	0.02047867	1.92889912
GO_STRUCTURAL_CONSTITUENT_OF_MUSCLE	0.01265662	1.87357571
GO_MYOFILAMENT	0.02718075	1.75936398
GO_MYOFIBRIL_ASSEMBLY	0.02047867	1.70005522
GO_ACTIN_MYOSIN_FILAMENT_SLIDING	0.04057227	1.66507122
GO_POSITIVE_REGULATION_OF_SMOOTH_MUSCLE_CELL_ PROLIFERATION	0.04630565	1.56071946

Table S3. List of GO pathways related to muscle differentiation commonly or differentially regulated in DM1 or non-DM1 cell lines from myoblasts to myotubes.

Abbreviations: NES: normalized enrichment score

common in DM1 and nonDM1		
pathway	**padj**	**NES**
GO_ACTIN_FILAMENT_BASED_MOVEMENT	0.0182555	1.84590055
GO_ACTIN_MEDIATED_CELL_CONTRACTION	0.0181814	2.19563341
GO_ACTIN_MYOSIN_FILAMENT_SLIDING	0.0181814	2.17862925
GO_ACTION_POTENTIAL	0.0182555	1.80776418
GO_ACTOMYOSIN_STRUCTURE_ORGANIZATION	0.02939984	1.61938644
GO_MUSCLE_CELL_DEVELOPMENT	0.01858137	1.68050193
GO_MUSCLE_CELL_DIFFERENTIATION	0.01985494	1.63851458
GO_MUSCLE_CONTRACTION	0.01960765	1.8034354
GO_MUSCLE_ORGAN_DEVELOPMENT	0.02014791	1.74404638
GO_MUSCLE_STRUCTURE_DEVELOPMENT	0.02126039	1.68710183
GO_MUSCLE_SYSTEM_PROCESS	0.01959137	1.80356905
GO_MUSCLE_TISSUE_DEVELOPMENT	0.031786	1.53735186
GO_MYOFIBRIL_ASSEMBLY	0.0181814	1.99425034
GO_MYOFILAMENT	0.0181814	1.7783661
GO_MYOSIN_II_COMPLEX	0.0181814	1.85943125
GO_REGULATION_OF_MUSCLE_SYSTEM_PROCESS	0.0313491	1.38870282
GO_SKELETAL_MUSCLE_ORGAN_DEVELOPMENT	0.01858137	1.60400751
GO_STRIATED_MUSCLE_CELL_DIFFERENTIATION	0.0313491	1.54769956
GO_STRIATED_MUSCLE_CONTRACTION	0.04783482	1.51151411
GO_STRUCTURAL_CONSTITUENT_OF_MUSCLE	0.0181814	2.07551241
only in nonDM1		
pathway	**padj**	**NES**
GO_ACTIN_FILAMENT_BUNDLE_ORGANIZATION	0.02500129	-1.7082806
GO_MESODERM_MORPHOGENESIS	0.03669841	-1.5419403
GO_POSITIVE_REGULATION_OF_ACTIN_FILAMENT_POLYMERIZATION	0.01180616	-1.8566163
GO_REGULATION_OF_ACTIN_FILAMENT_LENGTH	0.01180616	-1.6299536
GO_ACTIN_FILAMENT_BASED_PROCESS	0.01180616	1.52952967
GO_ACTININ_BINDING	0.04629302	1.63068784
GO_MUSCLE_FIBER_DEVELOPMENT	0.01180616	1.78597005
GO_MUSCLE_HYPERTROPHY	0.01180616	2.02477825

GO_MYOSIN_COMPLEX	0.01180616	1.76727751
GO_MYOSIN_FILAMENT	0.01180616	2.10635835
GO_POSITIVE_REGULATION_OF_SKELETAL_MUSCLE_TISSUE_DEVELOPMENT	0.042022	1.6967193
GO_REGULATION_OF_ACTIN_FILAMENT_BASED_MOVEMENT	0.02468595	1.76604176
GO_REGULATION_OF_MUSCLE_ADAPTATION	0.01180616	1.75761499
GO_REGULATION_OF_MUSCLE_CELL_DIFFERENTIATION	0.04185	1.41027052
GO_REGULATION_OF_MUSCLE_CONTRACTION	0.01180616	1.826582
GO_REGULATION_OF_MUSCLE_TISSUE_DEVELOPMENT	0.01916667	1.60113238
GO_REGULATION_OF_SKELETAL_MUSCLE_TISSUE_DEVELOPMENT	0.04496701	1.54391244
GO_REGULATION_OF_STRIATED_MUSCLE_CONTRACTION	0.01180616	1.84471796
GO_SKELETAL_MUSCLE_CELL_DIFFERENTIATION	0.01180616	2.02984286
GO_SKELETAL_MUSCLE_CONTRACTION	0.01180616	1.99822543
GO_STRIATED_MUSCLE_ADAPTATION	0.02468595	1.88461344
GO_ALPHA_ACTININ_BINDING	0.04619133	1.64472534

only in DM1

pathway	**padj**	**NES**
GO_MUSCLE_MYOSIN_COMPLEX	0.0181814	2.03464647

Table S4. Genes included in the heatmap in Figure 1E.

This heatmap includes the differential gene expression from hESC to Myoblast for the genes involved in the development of skeletal muscle, as listed in the Hallmark Myogenesis library of GSEA. The table and heatmap only include values for genes with an FDR<0.05. FC: log2 fold change, FDR: false discovery rate.

	Non DM1		DM1	
Gene	**Log2FC**	**FDR**	**Log2FC**	**FDR**
PGAM2	-7.6364474	0.00050996	-4.1372501	0.00228038
ACTN3	-7.1062215	0.00169109	-4.9963056	0.00141402
VIPR1	-6.684418	0.00011729	-6.5755281	1.1054E-05
GNAO1	-6.1910983	4.1641E-05	-6.0808602	1.0679E-07
ACTA1	-5.3121312	0.00459045		
KCNH2	-5.1236904	0.00183986	-2.6026062	0.01207283
MYH2	-5.0635294	0.00520164	-2.0813847	0.02477974
FXYD1	-4.8936168	0.00169415		
PTGIS	-4.5349603	0.00461408	-3.3097771	0.00055805
SORBS1	-4.204472	5.6523E-05	-3.193996	1.3774E-06
ERBB3	-3.8512355	0.00043801		
HRC	-3.6297947	0.01160065		
MYOZ1	-3.482335	0.00717859	-2.6183037	0.02848058
CACNA1H	-3.411508	0.00461981	-2.6953797	0.00109621
PYGM	-3.3522263	0.01775395		
GJA5	-3.0896497	0.00474154	-1.8749708	0.04047632
CKB	-2.8788679	0.00326882		
FGF2	-2.5262915	0.00955584	-3.2596399	0.00104467
CLU	-2.3593071	0.01343509	-1.3162698	0.0061474
SOD3	-2.2542128	0.02673005		
PTP4A3	-2.1849369	0.00643007	-1.1815027	0.04094168
SLC6A8	-2.0690044	0.0002861	-1.6167478	1.3472E-05
FKBP1B	-2.0080864	0.0059866	-2.0506157	5.2646E-06
SH3BGR	-1.8581192	0.01436419	-1.7977259	0.00025212
GPX3	-1.8481428	0.03745818	-2.3940478	0.00012671
FOXO4	-1.826665	0.0068506	-1.6908778	0.00308057
CFD	-1.7590589	0.03498819	-2.2272838	0.00151544
LARGE1	-1.3101683	0.00102905	-0.9173283	0.00416748
NOS1	-1.2629876	0.02469434		
LAMA2	-1.2051618	0.02739755		
HDAC5	-1.1630103	0.00354764	-0.8288821	0.00606047
ABLIM1	-1.1609756	0.0013776		
MYH11	-1.1157403	0.03127347		
FABP3	-1.0708169	0.04014091		
OCEL1	-0.9854368	0.02040891	-0.942291	0.00134744
DTNA	-0.9735365	0.01792914	-0.7680321	0.02640046

AGL	-0.6869365	0.03243653		
PFKM	-0.4816099	0.03997276		
SCD	-0.4237087	0.04357237		
BAG1	0.52291356	0.03661361		
TPM3	0.5531979	0.02759006		
SH2B1	0.63269704	0.01812807	0.65558606	0.00456142
SPTAN1	0.6420548	0.02553393	0.8783119	0.00133428
GABARAPL2	0.76464736	0.00303357	0.79314506	0.0011554
ITGB5	0.84040954	0.0433597	0.64552128	0.00101551
DMPK	0.93892448	0.03801914	2.33839218	0.00481972
CNN3	0.95240685	0.00765872	0.8327663	0.00028287
SORBS3	0.96911095	0.00389133	0.70863702	0.00207322
MEF2A	1.03887422	0.00189322	1.67415001	0.00167855
HSPB8	1.06612798	0.0461395		
MAPK12	1.1287699	0.00696582	0.71548276	0.00924735
MEF2D	1.21509755	0.00035714	1.45068928	0.00044345
CHRNB1	1.28042522	0.0279838	2.13804309	0.01104284
PKIA	1.30821332	0.00351101	1.57559488	6.2214E-05
MRAS	1.35782071	0.00285817	2.66211884	0.00114645
PLXNB2	1.42669337	0.00073714	1.30189246	1.2604E-05
RB1	1.50245783	0.00088596	1.37371906	6.5545E-05
CRAT	1.54450558	0.00122494	1.81393102	1.8562E-05
ACSL1	1.54936383	0.03491145	1.66672016	0.00069319
PPP1R3C	1.63281955	0.03958486	1.77194249	0.00447141
MYO1C	1.7080987	0.00099124	1.25387419	2.4556E-05
KLF5	1.74023751	0.00602375	2.91415737	0.00127289
GADD45B	1.74119308	0.00469833	1.49723194	0.01308782
AK1	1.78885198	0.00087464	1.99424536	0.00022705
BDKRB2	1.82705386	0.03652561	2.40704318	0.00141779
STC2	1.84520704	0.01910589	2.09760189	0.01258574
BIN1	1.88045433	0.00025973	2.67073101	0.0012023
AEBP1	1.88665576	0.00077659	1.4746003	0.00698089
IGFBP3	1.91990724	0.01449659	2.58270264	0.00037647
LPIN1	2.04999279	0.00011903	2.00339165	8.1572E-06
NCAM1	2.25890788	0.00478228	3.93859662	0.00028913
NQO1	2.30884621	0.00069818	2.07424127	0.00019916
SGCA	2.37896995	0.02383693	4.62772958	0.01354487
SIRT2	2.45797159	0.00028937	3.5285191	0.00035307
MYH3	2.50843605	0.02332573	6.95308417	0.00703814
PDLIM7	2.72154165	7.5496E-05	2.64355517	1.7823E-06
TPM2	2.80871992	0.00078469	2.93465456	8.1347E-06
MYLK	2.83151781	0.00443069	2.76635452	1.8483E-05
CTF1	2.87495473	0.00077659	2.47213046	0.00018835

MYH9	2.94513142	0.00015746	2.49330023	4.8667E-06
SVIL	3.01375511	0.00048534	2.95019569	7.4847E-08
COL4A2	3.04453224	0.00090295	2.78856241	5.8933E-05
TAGLN	3.06344378	0.00107551	1.87855956	0.00392026
ITGB1	3.0831708	0.00017315	2.60753692	7.4703E-06
GSN	3.09622146	0.0006844	3.52197322	3.2212E-05
SPARC	3.13473222	0.00019542	2.77060242	8.6243E-06
COL6A2	3.13819281	0.00077529	2.44537108	1.3031E-06
COL15A1	3.16355938	0.01475994	5.30371238	0.00108984
COL1A1	3.18915404	0.00104841	3.20779302	0.00025212
EPHB3	3.20310055	0.01904683	4.43428353	0.00073895
SMTN	3.27096114	0.00020537	2.63538877	1.0895E-05
MYLPF	3.31537411	0.01292004	7.21912669	0.00660378
SSPN	3.49300238	0.00029642	4.18483126	7.3464E-05
TGFB1	3.61486094	0.00163264	3.59273433	2.0195E-06
WWTR1	3.67345661	5.9126E-05	3.61272202	1.0047E-06
MYBPH	3.77887647	0.02689955	9.05159429	0.00545013
PRNP	3.96818459	0.00032957	3.45581746	1.0663E-05
KCNH1	3.97792156	0.00032767	4.612112	1.0941E-05
MEF2C	4.23754976	0.00011903	7.50750712	0.00047727
KIFC3	4.46366974	0.00106394	4.0230589	4.1261E-07
SPHK1	4.50026891	0.00011983	3.76449516	0.00044345
CDKN1A	4.51078872	0.00093463	3.45718467	0.00192736
HBEGF	4.53786655	0.00278658	3.48187621	0.00141428
LSP1	4.83654505	0.00989165	5.39217829	0.00094403
BHLHE40	4.86953754	0.00055626	3.84464037	2.5057E-05
MYOG	5.60690782	0.01467014	9.67484023	0.00227968
COL6A3	6.37157841	0.00048213	6.10605019	1.3089E-07
ADAM12	6.50025487	0.00017569	6.86283676	2.0486E-07
CDH13	6.52977417	0.00034417	6.0534943	1.6907E-06
SGCD	6.60504238	9.2577E-05	8.31569881	0.00036429
IGFBP7	7.86491015	0.00040475	7.40743712	1.35E-06
COL3A1	8.18258098	0.0037429	8.7579506	3.229E-06
MYL4	9.10699754	0.00855629	7.5034369	0.00370619
CHRNA1	9.43800137	9.337E-05	10.3710038	0.00016395

Table S5. Genes included in the heatmap in Figure 2D.

This heatmap includes the differential gene expression from Myoblast to Myotube for the genes involved in the development of skeletal muscle, as listed in the Hallmark Myogenesis library of GSEA. The table and heatmap only include values for genes with an FDR<0.05. FC: log2 fold change, FDR: false discovery rate.

	Non DM1		DM1	
Gene	**Log2FC**	**FDR**	**Log2FC**	**FDR**
LAMA2	3.434466542	0.004964119	2.558175579	0.002277686
COL3A1	2.969467392	0.042640266	2.955398545	0.003068552
DMD	2.767419811	0.009233199	2.785701929	0.003537978
SORBS1	3.356207514	0.010852453	2.837099843	0.004705953
IGF1	7.961961829	0.021266006	6.601104416	0.005055313
ABLIM1	2.032069952	0.007201063	1.303012396	0.006641053
GJA5	7.350950766	0.002335051	5.903106902	0.011650128
TSC2	0.588021565	0.022460709	0.513039783	0.011790923
ITGB5	-1.029597026	0.026519573	-1.095285801	0.011876489
CRYAB	4.338175471	0.034820232	4.160120198	0.012695223
KCNH2	6.514672136	0.005838995	4.339128578	0.012740782
FABP3	3.917470453	0.018246247	2.844873071	0.014690511
NQO1	-1.585215391	0.011538682	-1.701832158	0.016059109
SSPN	2.325759034	0.008582274	1.854418399	0.016346349
HSPB2	7.605691691	0.007093457	5.701880592	0.016384447
AGL	2.19265002	0.010213886	2.202678156	0.01644433
TGFB1	-1.4248959	0.01054286	-1.499853944	0.016523106
CKMT2	5.510813574	0.007047628	4.359050833	0.019705103
CD36	6.080426272	0.00316201	4.824471292	0.019878718
TCAP	3.558564383	0.032768447	3.69826496	0.021562269
ACHE	2.587647573	0.012991014	2.852586981	0.023164772
IGFBP3	2.158494815	0.038977168	2.034892733	0.024755399
SGCG	5.431689296	0.008587939	3.852361426	0.025090027
SPTAN1	0.891044981	0.026626872	1.02850752	0.025130091
MYL6B	2.271145922	0.005809485	2.011751398	0.025749356
FST	2.397183778	0.027555253	2.57317549	0.02608245
NAV2	0.932944466	0.043370045	1.452889679	0.02704499
FOXO4	2.35168128	0.01166004	2.003659929	0.027181795
PSEN2	2.464107869	0.010811335	2.214830878	0.02744485
SVIL	0.90121126	0.047568627	0.983028954	0.029391722
SPHK1	-2.711792186	0.014526251	-2.363562269	0.033438218
SLN	6.689599383	0.020011912	5.239655295	0.034400081
STC2	-1.878642266	0.021167168	-1.401806338	0.034646023
TNNC2	9.265908784	0.003587066	5.654457864	0.036055991
CACNG1	12.8305577	0.002038081	5.851439514	0.036566693
KLF5	3.317568511	0.005502216	2.267084435	0.036849485

MAPRE3	2.703345609	0.008206323	1.800803074	0.037299158
EIF4A2	0.538257268	0.015001838	0.523123553	0.03787702
COX6A2	7.460777533	0.026418018	4.278824389	0.038200662
PKIA	1.719028816	0.011076449	1.523168325	0.038819486
LDB3	6.076404982	0.004860348	3.719347159	0.039278995
SORBS3	-1.001467484	0.02041369	-0.550195828	0.041575078
SPEG	1.56457793	0.047736298	1.266826569	0.042457936
CAMK2B	3.697435383	0.021131387	2.620925713	0.04257657
TPM3	-1.116836487	0.007923713	-0.806040209	0.043181949
PRNP	-0.958295281	0.043240439	-0.911032826	0.04653724
CSRP3	5.176373525	0.015988941	3.822859929	0.049102734
MYL1	8.690728906	0.005249948	4.997857263	
ITGB1	-1.32925361	0.012021653	-0.956007405	
MYOM1	8.406506963	0.00437319	4.64701646	
MYOM2	6.149523336	0.009035857	3.951858259	
FXYD1	5.844446055	0.015558367	3.8650738	
TNNI2	8.721228713	0.00383752	4.527387147	
MRAS	2.93920966	0.002788993	1.814355448	
PFKM	0.53224965	0.029222214	0.651726107	
MYH7	7.370984742	0.010366123	4.306603954	
NCAM1	3.693855646	0.008582274	2.021400055	
DTNA	1.390336879	0.008571628	1.230408857	
DES	7.034624445	0.004698949	3.991609377	
CASQ2	8.629082168	0.005614601	4.269249435	
REEP1	4.211069025	0.021167168	2.801647477	
TNNT3	9.110154294	0.006431548	4.377343417	
MYL4	6.992537157	0.006402841	3.650003756	
MYH3	9.621307216	0.006432159	4.201878419	
ATP2A1	4.708730253	0.016644763	3.365619922	
ERBB3	5.219661863	0.003163749	2.760341145	
HRC	8.424311718	0.004502011	3.651198099	
CKM	10.24258556	0.004458363	4.58463117	
MEF2C	5.093576545	0.003993906	2.832725766	
ACTA1	8.031125266	0.002788993	3.735337947	
PTP4A3	1.812624089	0.038026673	1.23971904	
PC	1.488430115	0.039138238	1.195889434	
MYLPF	8.283638421	0.00437319	3.739768021	
CHRNG	5.137513774	0.007488854	2.445679116	
ACTN2	7.826633701	0.003473675	3.651630753	
MYH9	-1.273563434	0.016945518	-0.851558215	
MAPK12	-0.482987897	0.033912329	-0.528816105	
CAV3	7.610257638	0.003427943	3.225843372	
RYR1	6.04432954	0.014192291	3.044566438	

BIN1	1.795943956	0.008310537	1.383843173
SGCD	3.14043155	0.00437319	2.166361257
SGCA	4.713782962	0.00494004	2.798394202
SIRT2	1.737372248	0.006447267	1.332688915
PPFIA4	3.497203613	0.01497645	1.830181151
ENO3	4.48638605	0.013809202	2.260413772
LPIN1	-0.542167579	0.019825178	-0.382264166
MYH8	10.04747762	0.007033353	3.832054535
COL15A1	4.448857219	0.006614878	1.525656537
TNNT1	3.566188914	0.031091592	1.998472503
TNNT2	5.315065188	0.026132879	2.616352844
DMPK	1.680564158	0.005490022	1.129093845
TNNC1	7.914029201	0.002599395	2.770542097
ACTC1	6.249879394	0.011480179	2.758916827
TNNI1	6.175935646	0.016910263	2.458983265
CKB	3.613770376	0.008629059	1.788170616
MYBPH	8.177178805	0.009033672	2.769047414
CHRNB1	1.533927426	0.03392957	1.168247921
MYOG	6.047326723	0.018906755	2.385511018
MEF2D	0.522128005	0.015614808	0.391114879
SMTN	-0.985283507	0.03666777	-0.18946943

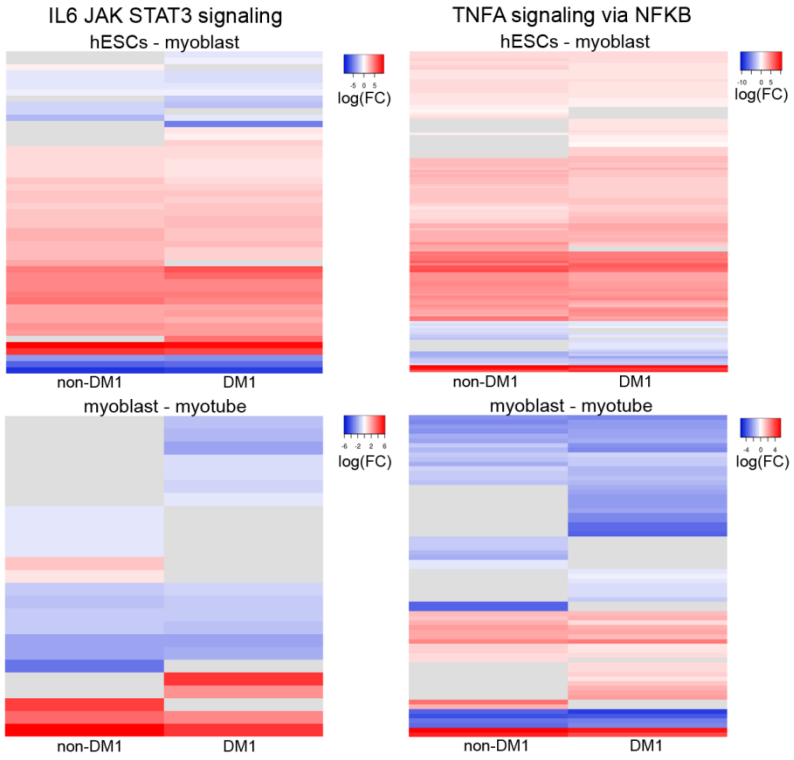

Fig. S3. Heatmaps representing the log fold change of genes belonging to IL6 JAK STAT3 signaling, and TNFA signaling via NFKB pathways.

Grey lines indicate genes with FDR>0.05. Abbreviation: NES: normalized enrichment score; FC: fold change.

Table S6. Genes included in the heatmaps in Figure 3B and Fig. S3.

Genes in the heatmap including the differential gene expression from stem cell to myoblast for the genes involved in the interferon alfa response, as listed in the Hallmark Interferon Alfa Response library of GSEA. The table and heatmap only include values for genes with an FDR<0.05. FC: log2 fold change, FDR: false discovery rate.

	Non DM1		DM1	
Gene	**Log2FC**	**FDR**	**Log2FC**	**FDR**
RTP4	-9.8710063	0.00293264	-9.1145961	6.7332E-06
BST2	-5.6689928	0.00255575	-3.711485	0.00012479
C1S	-3.6145526	0.00392271	-3.0921577	0.00013651
IFITM1	-3.783782	0.00072326	-2.6419353	9.8759E-05
DHX58	-2.6405175	0.00193729	-2.6029477	0.00179974
BATF2	-3.673551	0.0026175	-2.3881501	0.00069974
IFI30	-2.6087761	0.00148313	-2.033113	0.00088395
MX1			-1.2735789	0.01345829
OAS1	-0.9674436	0.00665148	-1.1838165	0.00029696
CD74	-1.9637571	0.00468261	-1.1216428	0.0034503
CCRL2			-0.9619376	0.03405482
TRIM14	-1.0517142	0.01177066	-0.838942	0.00210212
ADAR	-0.4538553	0.04326151	-0.5490263	0.02580798
PNPT1			-0.5315989	0.00552356
NUB1	0.52746854	0.0226403	0.32253053	0.01901764
CMTR1	0.31552143	0.0556944	0.35378361	0.00860065
LAP3	0.5442846	0.01821382	0.39143634	0.01018341
SLC25A28	0.66935904	0.03862344	0.50214236	0.00673699
OGFR			0.54021449	0.00991492
HLA-C			0.63838056	0.04410707
PARP12	0.89486011	0.01799961	0.69650345	0.00106813
TRIM5	0.86991497	0.00539115	0.69817181	0.01045006
TRIM25	0.72164805	0.00253848	0.76537427	0.00103142
NCOA7			0.8193937	0.0001103
CNP	0.91720551	0.00075643	0.93802208	9.2195E-05
TDRD7	0.97659574	0.03256812	0.98949348	0.00395936
MOV10			0.99001671	0.00089653
PARP14			1.03639898	0.00016168
IFIH1			1.07481521	0.04631453
PSME2	1.03072437	0.00182484	1.16555153	0.00026052
CASP8	1.68294852	0.00618372	1.18602132	0.00456825
TAP1	1.02090412	0.01523837	1.21394533	0.00147742
ELF1	0.95741278	0.03258727	1.3127996	4.2495E-06
IRF2	1.2394834	0.00328061	1.35173854	0.000708
STAT2	1.31630803	0.00361701	1.48633341	1.6408E-05
PSME1	1.04515988	0.00389609	1.52652453	0.00044223

CD47	1.69648427	0.00107538	1.60142131	0.00011415
LAMP3	1.90135588	0.00602392	1.60559618	9.7329E-05
EPSTI1			1.64657152	0.00390111
IL4R	1.69524039	0.00088818	1.65641998	5.886E-05
LGALS3BP	1.81575474	0.00880171	1.84981875	0.00021108
LPAR6	-2.1040376	0.00247152	1.8846873	0.00049018
DDX60	1.21449143	0.02815044	1.92595807	0.0004263
PSMB8	1.45747843	0.00678832	1.97870711	7.9371E-05
SP110	1.90136616	0.00273328	2.01496921	3.2379E-06
OASL			2.02315681	0.00013915
CMPK2	1.69994872	0.02669673	2.13970382	0.00022211
IFI35	1.66901342	0.02967756	2.29758269	0.00054942
IRF9	1.95929158	0.00064738	2.40028118	1.0354E-05
IL15	2.77078982	0.01500403	2.47188007	2.5073E-05
PSMB9			2.48831084	0.0018983
PARP9	2.17773954	0.00223631	2.82072021	1.4696E-05
RSAD2			2.87013131	0.00081155
CSF1	3.27242899	0.00057967	2.89144771	9.9354E-05
TENT5A	3.28138347	0.00159613	3.39027052	1.0692E-05
CXCL10	4.05629843	0.01356744	3.45304179	0.00127289
CXCL11	4.05629843	0.01356744	3.45304179	0.00127289
IRF1	3.11318206	0.00071388	3.51620023	2.9883E-07
B2M	3.41653854	0.00029518	3.79500874	4.6206E-06
IL7	4.26428611	4.1641E-05	4.14466523	3.2372E-07
IFIT3	3.44806214	0.00396568	4.14775246	2.8538E-06
IFIT2	3.24152066	0.01379642	4.24433006	4.4988E-06
GMPR	2.95956246	0.0048119	4.43908047	7.0662E-05
SAMD9	5.00413302	0.00100066	5.33463933	9.1734E-05
IFI27	4.68177109	0.00025745	5.34058862	8.8438E-07
UBA7	4.7775481	0.00262178	6.19323937	4.1436E-06
IFI44L	7.74855836	0.00460375	7.66551219	5.7307E-05
SAMD9L	8.38014829	0.00112005	7.69210855	2.9942E-05
GBP2	6.29738047	0.00556511	8.21587074	1.6461E-05
GBP4	8.02976632	4.1641E-05	8.87883336	3.3853E-08
IFI44	10.4740058	0.00215472	10.6670916	6.1887E-05
SELL	-1.086175	0.00286981		
TRIM21	0.84855874	0.01841346		
USP18	1.68356502	0.01309787		

Genes in the heatmap including the differential gene expression from myoblast to myotube for the genes involved in the interferon alfa response, as listed in the Hallmark Interferon Alfa Response library of GSEA. The table and heatmap only include values for genes with an FDR<0.05. FC: log2 fold change, FDR: false discovery rate.

	Non DM1		DM1	
Gene	**Log2FC**	**FDR**	**Log2FC**	**FDR**
TRIM25	-1.0161334	0.00407008	-1.2705931	0.00127928
PSMA3	-0.5968589	0.01195124	-0.6457465	0.00145744
CD47	-0.8292759	0.01368849	-0.8668103	0.03670892
GMPR	2.0767409	0.01461171		
USP18	1.02658003	0.0431299		
TRIM21	-0.5586301	0.04649472		
IL15			-1.2110939	0.00660677
IRF1			-2.2835597	0.00754558
PARP12			-1.0440708	0.00886797
CASP8			-0.8250892	0.00955576
PSME2			-0.9304172	0.01070195
IL4R			-0.8773788	0.01497536
OGFR			-0.5435969	0.02437785
IFI35			-1.6916088	0.02590576
PSMB8			-1.3500904	0.02745125
IFIT3			-1.4702349	0.0295467
MVB12A			-0.3519241	0.0317893
PLSCR1			-0.8445372	0.03327363
LGALS3BP			-1.3929268	0.03612207
EPSTI1			1.54308177	0.03908688
SP110			-0.6331772	0.04014417
CMPK2			-1.0556658	0.04543234
C1S			2.65304697	0.04649819
MOV10			-0.6852287	0.0495637

Genes in the heatmap including the differential gene expression from myoblast to myotube for the genes involved in the mTORC1 signaling, as listed in the Hallmark mTORC1 - Genes up-regulated through activation of mTORC1 complex- library of GSEA. The table and heatmap only include values for genes with an FDR<0.05. FC: log2 fold change, FDR: false discovery rate.

	Non DM1		DM1	
Genes	**Log2FC**	**FDR**	**Log2FC**	**FDR**
GGA2	1.39395718	0.00390196		
ERO1A	-1.3435659	0.00418508	-1.474942	0.0015409
CD9	-1.3961864	0.00437319		
ENO1	-1.6348037	0.0056941	-1.677491	0.00096568
EDEM1	-1.1586112	0.00640284		
EGLN3	5.14064024	0.00640284		
GAPDH	-1.2550856	0.00644727		
VLDLR	1.20587612	0.00663228		
AURKA	-1.7566402	0.00667111	-1.7725795	0.00289283
LDHA	-2.0607803	0.00744482	-2.1336723	0.0015409
TXNRD1	-0.7779018	0.00765844		
SRD5A1	-1.129161	0.00831054		
NUP205	-0.7874342	0.00831054		
SLC2A1	-1.7736938	0.00858794		
TFRC	-1.7180821	0.00874769	-1.3687902	0.00145744
SLC9A3R1	-1.034294	0.00900165		
GBE1	-1.2782428	0.00952393		
RRM2	-1.6230648	0.01001437	-1.8757533	0.00354383
PSMA3	-0.5968589	0.01195124	-0.6457465	0.00145744
FGL2	3.1913025	0.01259737		
BUB1	-1.7073953	0.01281787	-2.2026589	0.00129302
PLOD2	-1.3974453	0.01290488		
ACTR2	-0.7889837	0.01293796		
IDH1	-0.5842155	0.01375289		
BTG2	1.32461259	0.01461171		
PPIA	-0.7345603	0.01461171		
POLR3G	-1.3856651	0.01473787		
PNP	-2.150089	0.0157362		
EBP	-0.9706267	0.01614303		
DDX39A	-0.8585984	0.01625575		
MCM4	-0.9702213	0.01827781		
PSMD12	-0.6742016	0.01914544		
PSMD14	-0.7025409	0.01961858		
PSMC2	-0.4749448	0.0197571		
ACTR3	-0.8638794	0.02035067		
SLC6A6	-1.5638856	0.02065512		
PSME3	-0.5587381	0.02083138		

ACLY	-0.6157864	0.02083138		
TPI1	-0.7977651	0.02314094		
RPA1	-0.6340378	0.02484571	-0.7649368	0.00384886
FDXR	-0.903531	0.02518585		
MAP2K3	-1.334313	0.02557279	-1.1479065	0.00314594
CCT6A	-0.5660775	0.02613288		
MCM2	-1.0112654	0.02698042		
GLA	-1.1385406	0.02843371		
PSMD13	-0.5794091	0.02853326		
PSMG1	-0.6666482	0.02879422		
ADIPOR2	-0.4734363	0.0290815		
DHFR	-0.9707819	0.02926847		
PPA1	-0.7761836	0.0321806		
TUBG1	-0.9423582	0.03292739		
GSR	-0.7397882	0.0345282	-0.9562429	0.00246353
CCNF	-0.8882368	0.03460799	-1.3355966	0.00156703
GPI	-0.5971081	0.0347557		
ATP6V1D	-0.5788874	0.03599709		
CACYBP	-0.6562446	0.03629176		
UNG	-0.6598043	0.03632507		
PLK1	-1.8293413	0.03674075	-2.1954151	0.00204983
SORD	-0.510324	0.03801432		
INSIG1	-1.2541102	0.0389763		
GLRX	-0.9993069	0.03945555		
SLA	4.00791479	0.04056427		
CYP51A1	0.58406845	0.04186838	0.84543848	0.00175946
HSPE1	-0.6618585	0.04619077		
ETF1	-0.5282685	0.04631241		
CYB5B	-0.4931647	0.04649472		
AK4	-1.2301485	0.04649472		
CDC25A	-0.8583768	0.04848467		
EEF1E1	-0.6903684	0.04991954		
NAMPT			-1.2050141	0.00396463

Genes in the heatmap including the differential gene expression from myoblast to myotube for the genes involved in the canonical WNT signaling, as listed in the Hallmark WNT beta catenin signaling (Genes up-regulated by activation of WNT signaling through accumulation of beta catenin CTNNB1) library of GSEA. The table and heatmap only include values for genes with an FDR<0.05. FC: log2 fold change, FDR: false discovery rate.

	Non DM1		DM1	
Gene	**Log2FC**	**FDR**	**Log2FC**	**FDR**
DLL1	3.02490657	0.00357914		
PSEN2	2.46410787	0.01081134	2.21483088	0.02744485
NKD1	4.15693784	0.01546835	2.71488895	0.01281312
AXIN2	2.25386868	0.0160369	1.65954167	0.00394503
LEF1	2.33688891	0.01660013		
DKK1	-3.5601985	0.01701892		
SKP2	1.40983119	0.0191727		
WNT5B	-2.184473	0.02528114		
KAT2A	0.48746473	0.02801512		
JAG2	1.80956951	0.03902908		
GNAI1			0.4562088	0.02530757
TP53			-0.3964804	0.03756924
NUMB			-0.4112431	0.04817564

Genes in the heatmap including the differential gene expression from stem cell to myoblast for the genes involved in the IL6-JAK-STAT3 signaling, as listed in the Hallmark IL6-JAK-STAT3 signaling (Genes up-regulated by IL6 [GeneID=3569] via STAT3 [GeneID=6774], e.g., during acute phase response) library of GSEA. The table and heatmap only include values for genes with an FDR<0.05. FC: log2 fold change, FDR: false discovery rate.

	Non DM1		DM1	
Gene	**Log2FC**	**FDR**	**Log2FC**	**FDR**
IL6ST	4.26428611	4.1641E-05	4.14466523	3.2372E-07
OSMR	4.50750983	4.4035E-05	4.64246571	1.6061E-07
CD44	7.1533028	5.6523E-05	6.32644941	1.0077E-07
ITGA4	4.75482789	9.337E-05	5.98071831	3.5189E-07
PDGFC	5.0575846	9.8128E-05	4.33901364	1.0601E-07
IFNAR1	1.97760937	9.8973E-05	1.92092762	4.7556E-07
STAM2	1.92235282	0.00017136	1.83483037	5.6503E-07
PIK3R5	-7.9610759	0.00020256	-7.7903413	5.7319E-06
JUN	2.69348552	0.00021404	2.02752476	0.00287086
TYK2	1.80504095	0.00026724	1.86369814	9.7896E-08
IL1R1	4.41550369	0.00029969	5.28856073	5.135E-06
TNFRSF12A	2.33354197	0.00030757	1.71676477	0.00063839
ITGB3	9.29609163	0.00034365	8.69967984	1.0041E-05
CSF1	3.27242899	0.00057967	2.89144771	9.9354E-05
PTPN1	1.13157544	0.00061288	0.88953856	0.00071451
IRF9	1.95929158	0.00064738	2.40028118	1.0354E-05
IL10RB	2.54786608	0.00069408	2.35882848	1.5019E-05
IRF1	3.11318206	0.00071388	3.51620023	2.9883E-07
IL4R	1.69524039	0.00088818	1.65641998	5.886E-05
INHBE	-6.1033354	0.00111856	-5.6992855	0.00109621
SOCS3	1.88891489	0.00120972	2.59961308	0.00022229
TNFRSF1A	2.01843338	0.00144618	2.14672085	2.0286E-06
LEPR	1.23861536	0.00155782	1.23600981	0.0031101
TGFB1	3.61486094	0.00163264	3.59273433	2.0195E-06
IFNGR2	1.1425538	0.00211175	0.76948797	0.00090272
FAS	2.49815015	0.00237573	1.82850815	0.00316376
IL17RA	1.97799425	0.00313285	1.45886921	1.7864E-05
STAT2	1.31630803	0.00361701	1.48633341	1.6408E-05
CBL	-0.8496222	0.00384032	-1.0970443	5.335E-05
PTPN2	-0.7237833	0.0057656	-0.7274825	0.00011301
IL13RA1	3.12011256	0.00614545	3.26150887	9.4861E-07
CNTFR	-3.7908074	0.00658418	-4.4382957	0.00077272
TNFRSF1B	-2.9195845	0.00874089	-1.0890794	0.03153736
PIM1	-0.9760434	0.00962678	-1.3917178	0.00263493
TLR2	2.75568692	0.01338685	2.07934841	0.00118947
CXCL1	4.05629843	0.01356744	3.45304179	0.00127289

CXCL3	-1.5796414	0.01695678	-2.3876273	0.00531439
LTB	4.21479792	0.01856928	4.16486875	0.00101537
LTBR	-1.7181058	0.02377898		
IL17RB	-0.9959749	0.03588731	-1.2219837	0.00261062
PTPN11	0.45438024	0.04112286		
STAT1	1.26168843	0.04498209	1.01012492	0.00016363
TNFRSF21			0.71504354	0.00097337
BAK1			-0.62338	0.00460355
CSF2RA			-2.0893389	0.00515515
A2M			5.17346952	0.00537684
MYD88			0.86705336	0.01076212
CD9			-0.7455295	0.01546379

Genes in the heatmap including the differential gene expression from myoblast to myotube for the genes involved in the IL6-JAK-STAT3 signaling, as listed in the Hallmark IL6-JAK-STAT3 signaling (Genes up-regulated by IL6 [GeneID=3569] via STAT3 [GeneID=6774], e.g., during acute phase response) library of GSEA. The table and heatmap only include values for genes with an FDR<0.05. FC: log2 fold change, FDR: false discovery rate.

	Non DM1		DM1	
Gene	**Log2FC**	**FDR**	**Log2FC**	**FDR**
CD44	-2.431373	0.00233505	-2.1887476	0.00332717
CD36	6.08042627	0.00316201	4.82447129	0.01987872
CD9	-1.3961864	0.00437319	-1.3202866	0.00490647
TGFB1	-1.4248959	0.01054286	-1.4998539	0.01652311
PTPN1	-0.5990345	0.01400909		
CBL	-0.5498962	0.02630241		
HMOX1	-1.4525025	0.0280504	-1.010035	0.04107062
INHBE	3.42769504	0.03045296	2.91778296	0.01524444
A2M	4.59053439	0.03329534		
IL6ST	-0.6436064	0.03440211		
LEPR	-0.7105066	0.03478801		
TNFRSF12A	-1.6472052	0.03877374	-1.2299748	0.04556517
ITGA4	1.29781713	0.03945555		
STAT3	0.66499655	0.04262235		
ITGB3	-2.2464195	0.04905305	-2.4031601	0.04865699
ACVRL1			2.5921333	0.00238614
IL17RA			-0.8701443	0.00391008
IRF1			-2.2835597	0.00754558
TNFRSF21			-0.6900455	0.0103455
IL4R			-0.8773788	0.01497536
TNFRSF1A			-1.0208199	0.03128259

Genes in the heatmap including the differential gene expression from stem cell to myoblast for the genes involved in the TNFA signaling via NFKB, as listed in the Hallmark TNFA signaling via NFKB (Genes regulated by NF-kB in response to TNF [GeneID=7124].) library of GSEA. The table and heatmap only include values for genes with an FDR<0.05. FC: log2 fold change, FDR: false discovery rate.

	Non DM1		DM1	
Gene	**Log2FC**	**FDR**	**Log2FC**	**FDR**
IL6ST	4.26428611	4.1641E-05	4.14466523	3.2372E-07
PLAU	5.88192357	4.1641E-05	5.54780578	1.9938E-06
CD44	7.1533028	5.6523E-05	6.32644941	1.0077E-07
LIF	4.49126759	8.1067E-05	2.90652773	0.00127148
FOSL2	5.60709275	8.9611E-05	5.15794233	3.3853E-08
RELA	1.95923029	0.00010117	1.81292324	1.4451E-07
SPHK1	4.50026891	0.00011983	3.76449516	0.00044345
SERPINB8	4.668887	0.00013613	4.1179032	9.738E-07
SMAD3	3.01940803	0.00015057	3.22507329	3.5407E-07
TNC	7.19549432	0.00017773	6.53578839	7.8018E-07
B4GALT1	2.34716809	0.00018416	2.29763423	5.1062E-07
KLF2	5.86774385	0.00021367	3.44550138	0.00489474
CLCF1	4.95462355	0.00021385	4.50462716	3.0993E-05
JUN	2.69348552	0.00021404	2.02752476	0.00287086
IER3	4.61430028	0.00021548	4.16879302	7.4331E-06
GADD45A	2.37615749	0.00022834	1.77177622	0.00586905
INHBA	5.90445041	0.00025618	5.4155506	0.00139389
SPSB1	2.67608397	0.00025973	2.5137276	1.1426E-06
EGR2	-3.567657	0.00026586	-2.3488436	0.00229201
CCND1	3.62372926	0.00027331	1.99576619	0.00036472
DUSP4	4.99023601	0.00028991	6.56130903	1.3912E-05
PLAUR	4.37883786	0.00032423	3.75679352	4.6629E-05
PFKFB3	1.64385068	0.00040511	1.82839884	2.2004E-06
MAFF	3.04888309	0.00042883	2.47066841	0.00046907
TANK	1.47074501	0.0004501	1.51923592	2.3746E-06
PDLIM5	1.56274579	0.00053927	1.35287403	0.00049762
BTG3	1.34733034	0.0005397	0.93795034	0.0002928
BHLHE40	4.86953754	0.00055626	3.84464037	2.5057E-05
NR4A1	-3.5040709	0.00056571	-2.8485536	0.00020533
CSF1	3.27242899	0.00057967	2.89144771	9.9354E-05
FJX1	2.82362985	0.0006258	1.95049402	2.9199E-05
LDLR	1.40863979	0.00067307	0.93166494	0.00474641
PHLDA1	3.15350847	0.00068365	3.00703719	2.1122E-05
TIPARP	2.65146779	0.00068652	2.77018488	2.7692E-06
PLK2	4.18741038	0.00070396	4.16711182	3.1759E-06
IRF1	3.11318206	0.00071388	3.51620023	2.9883E-07
SERPINE1	7.33181838	0.00072915	5.88437571	0.00082336

SNN	-1.3941582	0.00075036	-1.2038017	8.5995E-05
PTX3	6.60548669	0.00081759	5.42035491	1.9576E-06
PTGS2	3.23038972	0.00081858	2.97712131	0.02046786
EHD1	2.15142068	0.00082951	1.8946288	4.3527E-05
FOSL1	5.48607244	0.00088633	3.8891711	0.00082335
CDKN1A	4.51078872	0.00093463	3.45718467	0.00192736
TNFAIP3	3.35810143	0.00095142	3.27851577	7.3386E-05
IER5	3.03155773	0.0009862	2.30612188	1.0126E-05
KLF6	2.59934461	0.00105975	2.33854264	1.8973E-05
RCAN1	3.84643829	0.00107611	3.13346514	0.00115921
BIRC3	4.56988422	0.00109641	4.81220036	4.2402E-05
PHLDA2	4.59568862	0.00114657	4.34233954	5.8592E-06
TGIF1	-1.2380713	0.00120375	-0.8684406	0.00210157
SOCS3	1.88891489	0.00120972	2.59961308	0.00022229
TNIP1	2.51333976	0.00121207	2.14218623	1.9077E-06
KLF10	1.53785774	0.00128274	1.43648325	0.00111541
LAMB3	4.56557751	0.00147924	2.17779783	0.00883152
NFKB1	2.91851395	0.00149282	2.20798068	9.4429E-07
PTGER4	2.98924487	0.0018416	3.64082741	2.8794E-05
BIRC2	1.19462475	0.00185609	0.96830537	9.1092E-05
LITAF	-2.1644054	0.00195738	-2.8840659	1.2199E-05
IFNGR2	1.1425538	0.00211175	0.76948797	0.00090272
MSC	3.58561922	0.00246516	4.85471623	1.9163E-05
TNFRSF9	9.73702815	0.00259861	7.74972642	2.2307E-06
KLF9	2.54511022	0.00262398	3.5627719	8.8011E-05
PMEPA1	2.34737165	0.00266264	2.0197655	0.00074986
ATP2B1	1.24963088	0.00268751	1.98921288	0.00381694
DUSP2	-3.3430403	0.00277126	-3.8870379	1.3395E-05
HBEGF	4.53786655	0.00278658	3.48187621	0.00141428
CEBPD	1.98691503	0.00282013	2.17173985	0.00025627
AREG	5.378497	0.00297827	5.40119768	8.2429E-05
BCL3	3.88778452	0.00318883	4.43261698	2.3507E-06
JUNB	2.49081017	0.0033155	2.99464106	4.8681E-07
NFIL3	1.3318753	0.00361713	1.14509689	4.451E-05
RHOB	1.99315782	0.00392704	1.25866895	0.02448467
MARCKS	1.4017005	0.00445957	1.27343242	6.8011E-06
GADD45B	1.74119308	0.00469833	1.49723194	0.01308782
IL7R	6.87695247	0.0047553	8.76481041	7.3636E-05
HES1	1.6312793	0.00484687	2.2504904	2.9199E-05
DENND5A	0.7961755	0.00494793	0.64816417	0.00124312
G0S2	3.73971023	0.00504929		
ICOSLG	-1.4611358	0.00516786		
IL1B	3.17661945	0.00604946		

DUSP1	2.85932912	0.00639778	2.66007103	0.00044989
DNAJB4	1.66752872	0.00646698	1.23238173	0.00204993
SLC2A3	-2.490632	0.00671404	-2.4354326	8.9969E-06
CCL2	3.52144505	0.00721261	4.27255331	6.1722E-05
DUSP5	2.04034973	0.00858352	1.13728097	0.01513775
VEGFA	2.34009207	0.00964687	2.04636415	0.00904804
SDC4	1.27702129	0.00983729		
PER1	-0.9487304	0.01014042	-0.5395033	0.01491049
NFE2L2	0.88435854	0.0105677	1.10888878	0.00011561
NFKBIA	1.12103951	0.01200224	0.74911493	0.008937
RELB	1.46356803	0.0120915	0.97011518	0.00947672
DRAM1	2.26758363	0.01284686	1.7168651	0.00818384
SQSTM1	1.19398864	0.01312401	1.23781692	0.00105948
TLR2	2.75568692	0.01338685	2.07934841	0.00118947
CXCL1	4.05629843	0.01356744	3.45304179	0.00127289
BTG2	1.63590986	0.01361685	1.50688623	0.0119254
IFIT2	3.24152066	0.01379642	4.24433006	4.4988E-06
GCH1	-1.9681908	0.01384497	-1.4944872	0.00673605
PPP1R15A	1.17026443	0.01386943	1.14940237	0.00805603
NFAT5	0.57650618	0.0146681	0.99085339	1.3572E-05
TAP1	1.02090412	0.01523837	1.21394533	0.00147742
CXCL3	-1.5796414	0.01695678	-2.3876273	0.00531439
SERPINB2	10.6075033	0.01786321	9.81919692	0.00049908
MAP2K3	0.94836477	0.01820229	0.80021588	0.00079607
IRS2	0.66352452	0.0193025		
GFPT2	-2.1920174	0.02142384	-1.0625651	0.02509286
TNFAIP8	1.54523973	0.02259913	0.99360976	0.01111727
SGK1	1.35289701	0.02295154	1.99890101	0.0004821
PTPRE	1.53770403	0.02818597	2.54723116	0.00010847
NFKB2	0.89019259	0.02965579		
SOD2	0.39954455	0.03543663		
MXD1	1.22740039	0.03689353	1.088996	0.01695058
EGR3	-2.5848334	0.04389306		
SIK1	1.8359086	0.04523988	2.79649665	0.01681219
EGR1	-1.4830135	0.04526919		
GEM	1.40099197	0.04571177	2.23244479	7.5245E-05
EIF1	0.47845916	0.04798672		
KDM6B			1.78397311	0.00029758
SAT1			1.19718371	0.00030512
PDE4B			-1.7775686	0.0005334
BTG1			1.89339298	0.00088351
TUBB2A			-0.866104	0.00658129
ZC3H12A			1.10377688	0.00917347

ICAM1	1.7576845	0.00997947
CD83	-1.1433299	0.01071153
TRIB1	-1.2813529	0.01164771
SLC2A6	0.66936924	0.0125713
TSC22D1	0.36656198	0.01316564
F3	1.34449689	0.02047407
ABCA1	1.11670153	0.02159121
PLPP3	-0.9462838	0.0289258
DDX58	0.63964827	0.02983679
CCNL1	0.30104418	0.03352216
CFLAR	1.144527	0.03471332
ZFP36	0.77305938	0.03667679
IFIH1	1.07481521	0.04631453

Genes in the heatmap including the differential gene expression from myoblast to myotube for the genes involved in the TNFA signaling via NFKB, as listed in the Hallmark TNFA signaling via NFKB (Genes regulated by NF-kB in response to TNF [GeneID=7124].) library of GSEA. The table and heatmap only include values for genes with an FDR<0.05. FC: log2 fold change, FDR: false discovery rate.

	Non DM1		DM1	
Gene	**Log2FC**	**FDR**	**Log2FC**	**FDR**
PLAU	-3.7253126	0.00233505	-4.4394853	0.00125701
CD44	-2.431373	0.00233505	-2.1887476	0.00332717
CCND1	-3.3758515	0.00256561	-2.854504	0.00652244
KDM6B	1.68461199	0.00278899	0.83548083	0.01987352
ICOSLG	3.06923682	0.00316375		
CEBPD	1.94083309	0.0045315	1.3928021	0.00705977
IL1B	-3.6097374	0.00472061	-3.4161109	0.03199129
EGR2	5.52392201	0.00500721	4.88603149	0.00088082
IER3	-1.9627713	0.00643155		
SERPINB8	-2.0400797	0.00644727	-1.8445558	0.01123286
PLAUR	-3.2580499	0.00728704	-3.0088861	0.00459787
PFKFB3	-1.2937208	0.00774095	-1.5452674	0.00185298
FOSL1	-4.1635059	0.00782501	-3.9771904	0.00085706
SPSB1	-1.2978482	0.00889246		
PER1	0.93214356	0.00941864	0.64116797	0.02365818
ATP2B1	1.71999824	0.01161296		
ZBTB10	0.99628161	0.01183729	0.65840089	0.02068093
PHLDA2	-2.2567037	0.01220746	-2.3755433	0.0089609
ETS2	-0.977517	0.01231359	-1.5892265	0.00404488
VEGFA	-2.5958891	0.01331465	-2.7326907	0.0098362
SPHK1	-2.7117922	0.01452625	-2.3635623	0.03343822
BTG2	1.32461259	0.01461171	1.57064958	0.01837678
MSC	2.13075635	0.0198375	1.73099421	0.0266424
KLF9	-1.7512155	0.0200161	-2.7091698	0.00120837
IRS2	-1.297685	0.02116717	-1.0150547	0.01926929
MAP2K3	-1.334313	0.02557279	-1.1479065	0.00314594
EGR1	2.4955646	0.02913575	2.70121992	0.0043867
PHLDA1	-1.1342375	0.02995247	-1.7543035	0.00278674
DENND5A	-0.5718393	0.03011756		
TNC	1.32976083	0.03011893	1.34942421	0.03199123
LIF	-1.8109141	0.03025927	-2.0833327	0.02430623
EGR3	4.79107308	0.03266606	3.77781214	0.00320201
SAT1	-1.4657417	0.03412257	-1.6196244	0.02090836
IL6ST	-0.6436064	0.03440211		
SNN	0.70054093	0.0362185	0.68996913	0.04236406
BCL6	0.75612844	0.03683152		
ID2	-1.1352427	0.03709973		

SERPINE1	-3.6072948	0.03771482		
MAFF	-1.8013523	0.03798174	-1.2231861	0.04833985
SDC4	-1.2388338	0.04039827		
INHBA	-1.5555937	0.04132073		
DUSP4	-1.1872072	0.04208609	-2.4941912	0.00384886
NR4A1	1.92101262	0.04405169	1.87336331	0.01163682
G0S2			-3.5975766	0.00363902
NAMPT			-1.2050141	0.00396463
IRF1			-2.2835597	0.00754558
DUSP2			2.13306166	0.00955576
FJX1			0.73479925	0.01074221
ABCA1			-2.1740011	0.01153193
BCL3			-1.9951603	0.01227016
TNIP1			-0.7465809	0.0151081
B4GALT5			-0.61299	0.01746993
AREG			-3.4324499	0.01751988
SQSTM1			-0.8575789	0.01933262
LAMB3			-2.2413078	0.02108977
SLC2A6			-0.8473012	0.02108977
NR4A3			1.86056543	0.02689223
KLF2			1.22503553	0.02836673
TRIP10			-0.3918087	0.0300163
TNF			1.34942421	0.03199123
TUBB2A			0.78802077	0.03437131
F2RL1			-2.8280786	0.03625759
NFAT5			-0.4541473	0.03787702
GFPT2			-2.2206588	0.04171543
CDKN1A			1.68918886	0.04173948
RHOB			0.52301439	0.04269738
PDLIM5			0.90131606	0.04302633

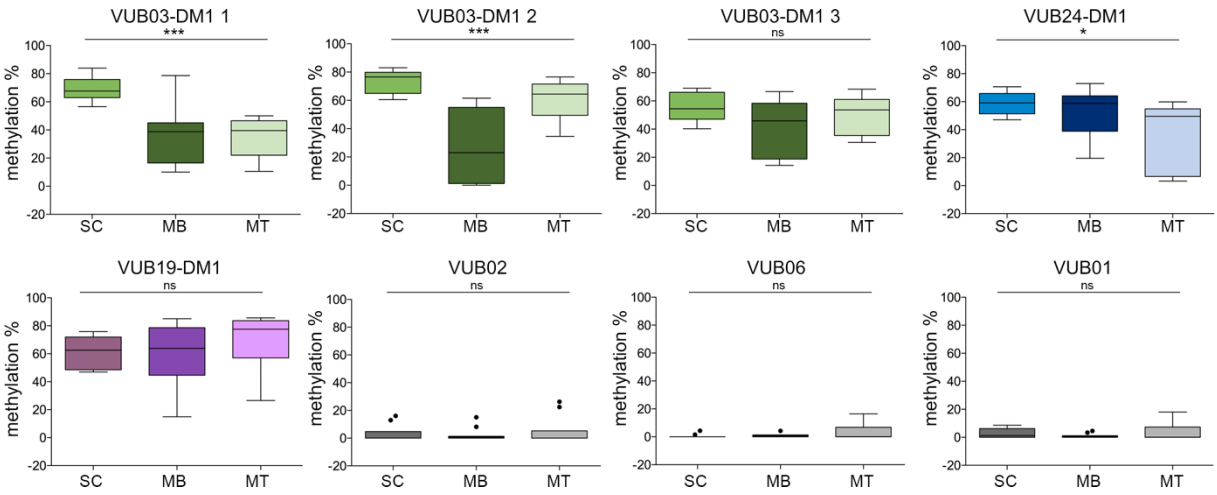

Fig. S4. The CpG methylation downstream of the CTG repeat in DM1 samples and non-DM1 samples over the course of differentiation.

The downstream methylation is shown for 11 CpG sites after massive parallel sequencing for 3 DM1 and 3 non-DM1 cell lines. The methylation status of the downstream region decreases for some lines (One-way Anova VUB03-DM1 1 and 2 $p<0.0001$, VUB24-DM1 $p= 0.0214$) other lines remain unchanged (One-way Anova VUB03-DM1 3 $p=0.0913$, VUB19-DM1 $p=0.4399$, VUB02 $p=0.5037$, VUB06 $p=0.0753$, VUB01 $p=0.2927$). Abbreviations: SC: hESC; MB: myoblasts; MT: myotubes

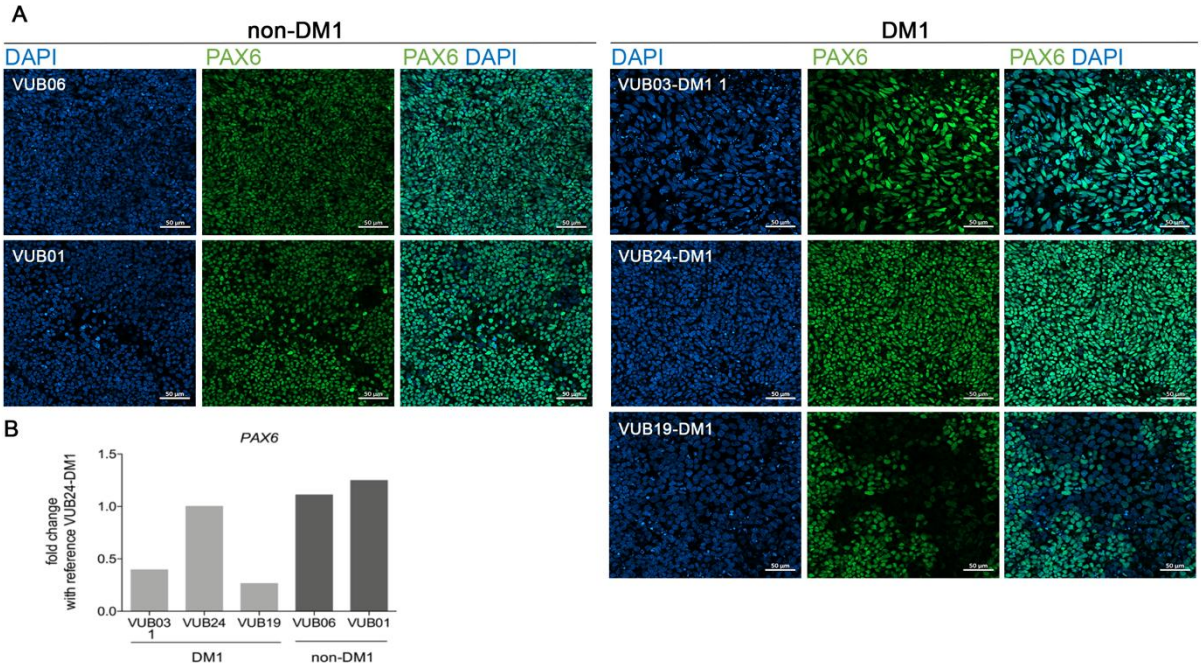

Fig. S5. Characterization of the cells after neuroectoderm differentiation.

(A) Immunostaining for the neuroectoderm marker PAX6 for 2 control non-DM1 cell lines and 3 DM1 cell lines after 12 days of neuroectoderm differentiation. **(C)** *PAX6* mRNA expression neuroectoderm cells relative to the DM1 reference sample VUB24. *UBC* and *GUSB* gene expression was used for normalization. The experiment was only performed once.

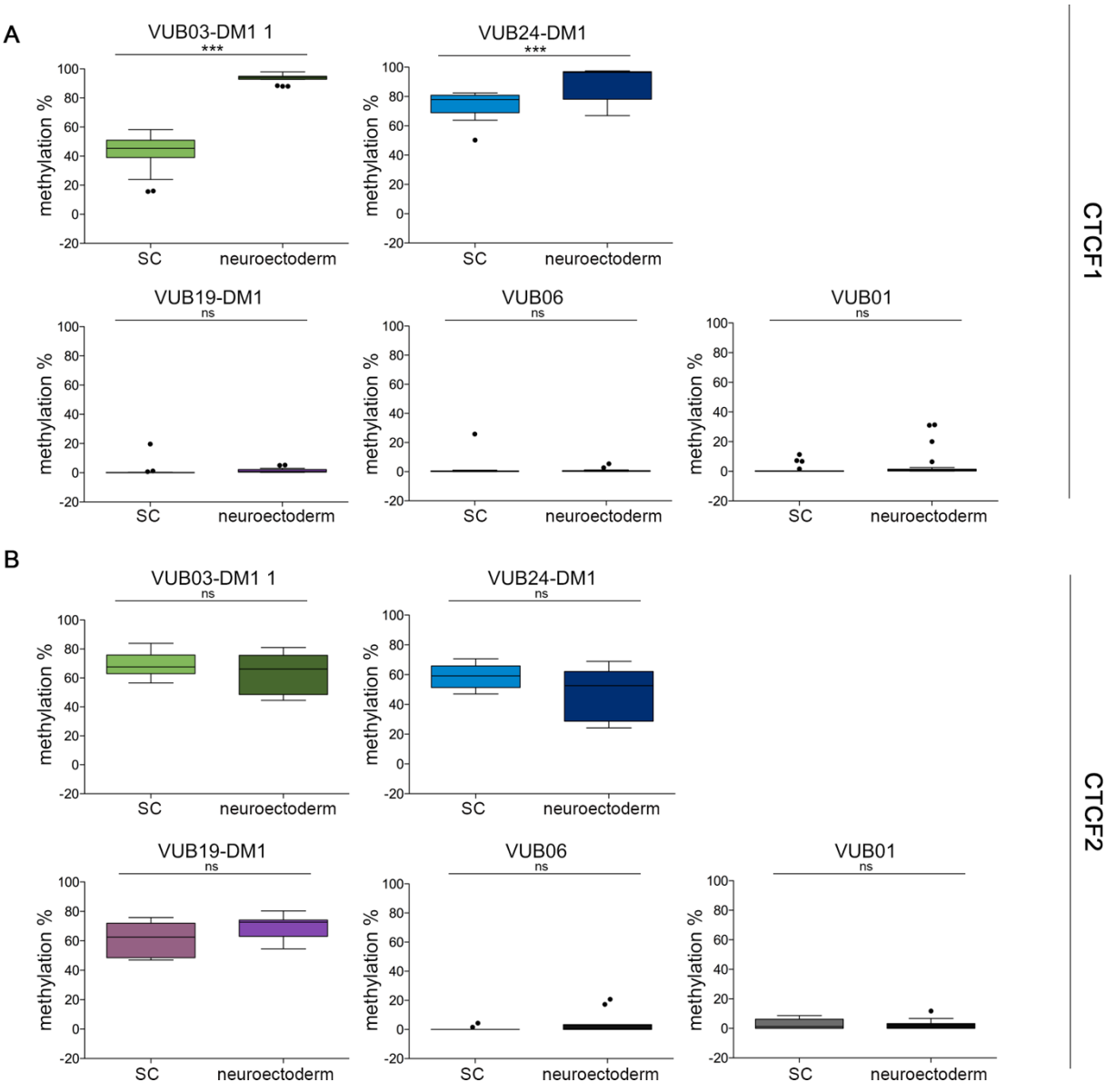

Fig. S6. The upstream CpG methylation tends to increase over neuroectoderm differentiation in DM1 samples, the downstream CpG region remains unchanged.

(A) Methylation levels of the CpG sites upstream of the CTG repeat. The upstream methylation is shown for 23 CpG sites and all epi-alleles were analyzed after massive parallel sequencing for 3 DM1 cell lines and 2 non-DM1 cell lines (one-way Anova). **(B)** Methylation levels of the CpG sites downstream of the CTG repeat. The upstream methylation is shown for 23 CpG sites and all epi-alleles were analyzed after massive parallel sequencing for 3 DM1 cell lines and 2 non-DM1 cell lines (one-way Anova).

Table S7. Splicing defects comparing DM1 myoblasts versus myotubes
https://figshare.com/s/491658bfa49266b27e9a

Table S8. Splicing defects comparing DM1 stem cells versus myotubes
https://figshare.com/s/491658bfa49266b27e9a

Table S9.: Splicing defects comparing non-DM1 lines versus VUB03_DM1
https://figshare.com/s/491658bfa49266b27e9a

Table S10.: Splicing defects comparing non-DM1 myotubes versus DM1 myotubes
https://figshare.com/s/491658bfa49266b27e9a

Table S11. Splicing comparing non-DM1 myotubes versus non-DM1 myotubes
https://figshare.com/s/491658bfa49266b27e9a

Table S12. Splicing defects comparing non-DM1 myotubes versus DM1 myotubes
https://figshare.com/s/491658bfa49266b27e9a

Table S13.: Splicing defects comparing non-DM1 stem cells versus DM1 stem cells
https://figshare.com/s/491658bfa49266b27e9a

Table S14. Splicing comparing non-DM1 stem cells versus non-DM1 myotubes
https://figshare.com/s/491658bfa49266b27e9a

Table S15. Probes, assays and primers for qRT-PCR.

Gene	**TaqMan Assay/ Sequence**
MYOG	Hs01072232_m1
MYOD1	Hs00159528_m1
IL6	Hs00174131_m1
TRL3	Hs01551079_g1
IRF7	Hs01014809_g1
PAX6	Hs00240871_m1
GUSB	Hs99999908_m1
UBC	Forward 5'-CGCAGCCGGGATTTG-3' Reverse 5'-TCAAGTGACGATCACAGCGA-3' Probe 6-FAM-TCGCAGTTCTTGTTTGTG-MGB
GAPDH	Forward 5'-ATGGAAATCCCATCACCATCTT-3' Reverse 5'-CGCCCCACTTGATTTTGG-3' Probe 6-FAM-CAGCAGCGAGATCC-MGB

Table S16. List of used antibodies and manufacturers.

Primary antibodies	**Species**	**Application**	**Company**	**Cat#**
HNK-1-FITC (B3GAT1)	Mouse	FACS	AVIVA SYSTEMS BIOLOGY	OASA02271
C-MET-APC (anti-HGF R/C-met)	Mouse	FACS	R&D systems	FAB3582A
MF20	Mouse	ICC	DSHB	NS
PAX6	Mouse	ICC	Abcam	ab78545
Secondary antibodies	**Species**	**Application**	**Company**	**Cat#**
Alexa Fluor 488	Goat-anti-Mouse	ICC	Invitrogen	A11001

Table S17. List of primers.

Primer sequences for the amplification and massive parallel sequencing of CTCF1 and CTCF2. 'F' indicates the forward primers, 'R' the reverse primers. Number '1' following 'F' or 'R' indicate the first round of the nested PCR. For the second PCR round, primers with Miseq at the end of the target name were used.

Target name	**Primer sequence**
CTCF1 F1	5'-TGTYGTYGTTTTGGGTTGTATTG-3'
CTCF1 R1	5'-CAACATTCCYGACTACAAAAACCCTT-3'
CTCF2 F1	5'-TTYGGTTAGGTTGAGGTTT-3'
CTCF2 R1	5'-TTAACAAAAACAAATTTCCC-3'
CTCF1 F Miseq	5'-TCGTCGGCAGCGTCAGATGTGTATAAGAGACAGGTTGTATTGGGTTGGTGGTTTA-3'
CTCF1 R Miseq	5'- GTCTCGTGGGCTCGGAGATGTGTATAAGAGACAG CTACAAAAACCCTTYGAACCC-3'
CTCF2 F Miseq	5'-TCGTCGGCAGCGTCAGATGTGTATAAGAGACAGTAAATTGTAGGTTTGGGAAG-3'
CTCF2 R Miseq	5'-GTCTCGTGGGCTCGGAGATGTGTATAAGAGACAGTTAACAAAAACAAATTTCCC-3'
DM101	5'-CTTCCCAGGCCTGCAGTTTGCCCATCCA-3'
DM102	5'-GAACGGGGCTCGAAGGGTCCTTGT-3'